Automatica 176 (2025) 112266

Contents lists available at ScienceDirect

Automatica

journal homepage: www.elsevier.com/locate/automatica

Output-feedback event-triggered boundary control of reaction–diffusion PDEs with delayed actuator☆

Hongpeng Yuan, Ji Wang *, Jianping Zeng, Weiyao Lan

Department of Automation, Xiamen University, Xiamen 361005, China

ARTICLE INFO

Article history:
Received 1 June 2024
Received in revised form 24 October 2024
Accepted 6 February 2025

Keywords:
Reaction–diffusion PDE
Boundary control
Backstepping
Delay-compensated control
Event-triggered control

ABSTRACT

We present an output-feedback event-triggered delay-compensated boundary control scheme for a class of reaction–diffusion PDEs under a delayed actuator, where an arbitrarily long time delay exists between the PDE plant and the ODE actuator. After treating the time delay as a transport PDE, the overall plant configuration becomes ODE-PDE-PDE. Combining the PDE and ODE backstepping designs, a three-step backstepping transformation is proposed to build the continuous-in-time control law. A PDE observer is designed to track the PDE states required in the control law using a boundary measurement. Then, a dynamic event-triggering mechanism is designed, based on the evaluation of the overall ODE-PDE-PDE system, to determine the updating times of the control signal. In the resulting output-feedback event-based closed-loop system, a strictly positive lower bound of the minimal dwell time is found, which is independent of initial conditions. As a result, the absence of a Zeno behavior is guaranteed. Besides, exponential convergence to zero of all signals is proved via Lyapunov analysis, including the H^1 norm of the transport PDE state, the L^2 norm of the reaction–diffusion PDE and observer states, the actuator states, the internal dynamic variable in the event-triggering mechanism, as well as the control input. The effectiveness of the proposed method is illustrated by numerical simulation.

1. Introduction

1.1. Boundary control of reaction–diffusion PDEs

Reaction–diffusion systems are utilized to describe various physical models in the areas of biology, ecology, physics, and chemistry, playing a very important and extensive role in these fields (see e.g. Desvillettes, Fellner, and Bao (2017), Grindrod (1991), Holmes, Lewis, Banks, and Veit (1994), Ivancevic and Ivancevic (2008), Nagahara and Yanagida (2018)). In the past two decades, numerous studies have been conducted on the control of reaction–diffusion PDEs. The basic control designs can be found in Krstic and Smyshlyaev (2008b). Besides, some extended results have been presented considering the additional effects that exist in the reality of applications, such as perturbation (Baccoli, Pisano, & Orlov, 2015), nonlinearities (Krener, 2022), actuator dynamics (Deutscher & Gehring, 2020; Li, Wu, & Wen, 2021) and so on. In this paper, for a class of reaction–diffusion PDEs, we will deal with the effect of time delay that often exists in practical control systems, and propose a more user-friendly triggering-type controller whose input is piecewise constant.

1.2. Delay-compensated boundary controls of PDEs

The boundary control of PDEs subject to time delays has been extensively studied in the past more than ten years. For instance, Auriol, Aarsnes, Martin, and Di Meglio (2018), Auriol, Bribiesca Argomedo, Saba, Di Loreto, and Di Meglio (2018) proposed delay-robust control laws for coupled hyperbolic PDEs, where the robustness with respect to a small delay is considered. Going beyond this, for the purpose of compensating for arbitrarily long delays, a delay compensation technique (Krstic, 2009b), where the delay is captured as a transport PDE, has been applied to PDE delay-compensated control. By this technique, a delay-compensated control law for a class of reaction–diffusion PDEs with an input delay was presented in Krstic (2009a), and extended to the case of unknown input delay in Wang, Qi, and Diagne (2021). Besides, this delay-compensation technique has also been implemented in other types of PDEs or nonlinear systems, e.g., Burns, Herdman, and Zietsman (2013), Diagne,

☆ This work was supported by the National Natural Science Foundation of China under Grant 62203372. The material in this paper was partially presented at The 63rd IEEE Conference on Decision and Control (CDC), December 16–19, 2024, Milan, Italy. This paper was recommended for publication in revised form by Associate Editor Mamadou Diagne under the direction of Editor Miroslav Krstic.

* Corresponding author.
E-mail addresses: 23220221151757@stu.xmu.edu.cn (H. Yuan), jiwang@xmu.edu.cn (J. Wang), jpzeng@xmu.edu.cn (J. Zeng), wylan@xmu.edu.cn (W. Lan).

https://doi.org/10.1016/j.automatica.2025.112266

Bekiaris-Liberis, Otto, and Krstic (2017a, 2017b), Katz, Fridman, and Selivanov (2021), Koga, Bresch-Pietri, and Krstic (2020), Lhachemi, Shorten, and Prieur (2019), Wang and Krstic (2020), Zhu, Krstic, and Su (2018). Treating the parabolic PDE with the input delay as a parabolic PDE cascaded with a transport PDE, it makes the control design belong to the boundary control problem of a class of hyperbolic–parabolic PDEs, which has been dealt with in recent contributions (Chen, Vazquez, Liu, & Su, 2023; Deutscher, Gehring, & Jung, 2023). However, they only employ continuous-in-time approaches while we pursue a more user-friendly control law in the event-triggering framework and incorporate the additional actuator dynamics in this paper.

1.3. Event-triggered boundary controls of PDEs

Event-triggered control (ETC) is a control implementation technique where the control input is updated aperiodically (only when necessary), which is different from the periodic sampled-data control. Over the past decade, many significant ETC results have been reported for the systems described by linear or nonlinear ordinary differential equations (ODEs), e.g., Donkers and Heemels (2012), Heemels, Donkers, and Teel (2013), Marchand, Durand, and Castellanos (2013), Postoyan, Tabuada, Nešić, and Anta (2015), Zhang, Liu, and Jiang (2021). However, when it comes to the ETC of PDE, the results are less, as this topic has been under investigation for a much shorter period than ODE ETC. Some notable ETC works developed for PDEs can be seen in Espitia, Girard, Marchand, and Prieur (2018), Espitia, Karafyllis, and Krstic (2021), Wang and Krstic (2022b, 2023) for state-feedback form and Espitia (2020), Rathnayake and Diagne (2024), Rathnayake, Diagne, Espitia, and Karafyllis (2022), Rathnayake, Diagne, and Karafyllis (2022), Wang and Krstic (2022c) for output-feedback control, with applications in traffic control, re-entrant manufacturing systems, and Stefan problem, shown in Diagne and Karafyllis (2021), Espitia, Auriol, Yu, and Krstic (2022), Koga, Demir, and Krstic (2023), Rathnayake and Diagne (2023b), respectively. Besides, some novel periodic and self-triggered components in event-based control for PDEs have also been proposed in Rathnayake and Diagne (2023b, 2023c, 2024) recently for parabolic PDEs. The above event-triggered control designs for reaction–diffusion PDEs assume that the actuation directly affects the PDE boundary. However, in particular physical applications, the actuation signal does not have direct access to the PDE boundary and is instead implemented through an actuator, which, be it hydraulic or electrical, has its own considerable inertia, namely its own lumped-parameter dynamics modeled by an ODE. For instance, in the control of a thermal system like the Stefan PDE, the actuation does not directly access the boundary of the heat flux, but is instead carried out with an electrical actuator whose input is the voltage that drives the heater through an RC series circuit (Koga et al., 2020). Moreover, in some cases, e.g., the cases of antennas for nuclear fusion (Argomedo, Witrant, & Prieur, 2014) or sprays for surface decontamination (Wang, Diagne, & Qi, 2021), the actuation generated from the actuator does not act on the considered PDEs immediately, rendering a time delay between the actuator and PDE model. This delay could be due to network effects, the physical properties of the actuator, the physical distance between the actuator and the plant, and so on.

In this paper, considering actuator dynamics and the delayed actuation to the reaction–diffusion PDE plant, we propose an observer-based output-feedback event-triggered boundary control design for a class of reaction–diffusion PDEs.

1.4. Contributions

(1) In comparison to Rathnayake, Diagne, Espitia, et al. (2022) regarding output-feedback event-triggered backstepping control for parabolic PDEs, we incorporate the delayed actuator dynamics in this paper.
(2) Different from delay-compensated event-triggered boundary control designs of hyperbolic PDEs in Wang and Krstic (2022a), in this paper, the considered PDE model is a class of reaction–diffusion PDEs.
(3) To the best of our knowledge, the first and sole result on the event-triggered delay-compensated boundary control of reaction–diffusion PDEs is recently presented in Koudohode, Espitia, and Krstic (2024), which achieves the exponential stability with supremum norm of the delay state by using the small-gain approach. In our work, the exponential convergence of all signals in the closed-loop system is guaranteed, including H^1-norm for the delay state, by using Lyapunov analysis that has broader applicability to other type systems. Additionally, we incorporate the actuator dynamics in the control design. It is beneficial to exclude the discontinuities in the domain of the delay PDE as the actuator ODE actually acts as a low-passing filter but causes difficulties in the control design, considering the higher-order control input and additional actuator states need to be regulated to zero in the event-based closed-loop system. Besides, the full-state feedback control is designed in Koudohode et al. (2024) while the output-feedback controller is built in our paper.
(4) The first output-feedback control result of the ODE–delay PDE–reaction–diffusion PDE cascade is present in Lhachemi and Shorten (2023), where a finite-dimensional control design is proposed by leveraging the spectral reduction method. Different from Lhachemi and Shorten (2023), we conduct the control design based on the original infinite-dimensional model directly, and moreover, our control signal is in a piecewise fashion by designing a triggering mechanism, which represents an improvement over Lhachemi and Shorten (2023) that used a continuous-in-time approach.

1.5. Notation

We adopt the following notation.

(1) The symbol $\mathbb{N}$ denotes the set of natural numbers including zero, and the notation $\mathbb{N}^*$ for the set $\{1, 2, \ldots\}$, i.e., the natural numbers without 0. We also denote $\mathbb{R}_+ := [0, +\infty)$ and $\mathbb{R}_- := (-\infty, 0)$.
(2) Let $U \subseteq \mathbb{R}^n$ be a set with non-empty interior and let $\Omega \subseteq \mathbb{R}$ be a set. By $C^0(U; \Omega)$, we denote the class of continuous mappings on U, which takes values in Ω. By $C^k(U; \Omega)$, where $k \geq 1$, we denote the class of continuous functions on U, which have continuous derivatives of order k on U and take values in Ω.
(3) We use the notation $f[t]$ (e.g., u, v) to denote the profile of f at certain $t \geq 0$, i.e., $(f[t])(x) = f(x, t)$.
(4) Given an open set Ω, $L^2(\Omega) = \{u : \Omega \to \mathbb{R}; \int_\Omega |u(x)|^2 dx < +\infty\}$ endowed with the norm: $\|u\|^2 = \langle u, u\rangle = \int_\Omega |u(x)|^2 dx$, and $H^1(\Omega) = \{u \in L^2(\Omega); u_x \in L^2(\Omega)\}$ endowed with the norm $\|u\|^2_{H^1(\Omega)} = \|u\|^2 + \|u_x\|^2$. The single bars $|\cdot|$ for $X(t)$ denote the Euclidean norm if $X(t) \in \mathbb{R}^n$.
(5) The symbol $e_{i,j} (i, j \in \mathbb{N}^*)$ means a j-dimensional vector where the ith entry is 1 and the other entries are 0.
(6) Define $\underline{x}_i^T := [x_1, \ldots, x_i]$, and $\underline{y}_i^T := [y_1, \ldots, y_i]$.

2. Problem formulation

Consider the following plant

$$u_t(x,t) = \varepsilon u_{xx}(x,t) + \lambda u(x,t), \tag{1}$$
$$u(0,t) = 0, \tag{2}$$
$$u(1,t) = CX(t-D), \tag{3}$$
$$\dot{X}(t) = A_n X(t) + e_{n,n} U(t), \tag{4}$$

$\forall (x,t) \in [0,1] \times [0,\infty)$, where $U(t)$ is the control input to be designed, $u(x,t)$ is the state of the reaction–diffusion PDE and $X(t) = [x_1, x_2, \ldots, x_n]^T$ is the state of the ODE describing the actuator dynamics ($n \in \mathbb{N}$ and $n > 1$). There exists a time delay D, whose length is arbitrary, in the transmission of the actuation signal generated by the actuator to the PDE plant. Define matrices A_i ($i \le n, i \in \mathbb{N}^*$), which will be used later, as

$$A_i = \begin{pmatrix} a_{1,1} & 1 & 0 & \ldots & 0 \\ a_{2,1} & a_{2,2} & 1 & \cdots & 0 \\ & & \vdots & & \\ a_{i-1,1} & a_{i-1.2} & \ldots & a_{i-1,i-1} & 1 \\ a_{i,1} & a_{i,2} & \ldots & a_{i,i-1} & a_{i,i} \end{pmatrix}, \tag{5}$$

and the system matrix A_n in (4) is the one with $i = n$ in (5). The n-dimensional vectors C, $e_{n,n}$ in (3), (4) are

$$C = [1, 0, \ldots, 0], \quad e_{n,n} = [0, 0, \ldots, 1]^T. \tag{6}$$

The distributed state $u(x,t)$ of the PDE plant is unmeasurable. The PDE plant parameters λ, ε are positive.

Remark 1. An eigenfunction expansion of the solution of (1)–(3) with the boundary value $x_1(t) = 0$ shows that the parabolic PDE system is unstable when $\lambda > \varepsilon\pi^2$.

According to Krstic (2009a), introducing a new variable

$$v(x,t) = x_1(t + x - 1 - D),$$

we rewrite the system (1)–(4) as:

$$u_t(x,t) = \varepsilon u_{xx}(x,t) + \lambda u(x,t), \quad x \in (0,1) \tag{7}$$
$$u(0,t) = 0, \tag{8}$$
$$u(1,t) = v(1,t), \tag{9}$$
$$v_t(x,t) = v_x(x,t), \quad x \in (1, 1+D) \tag{10}$$
$$v(1+D,t) = x_1(t), \tag{11}$$
$$\dot{X}(t) = A_n X(t) + e_{n,n} U(t), \tag{12}$$

which is a system of ODE-PDE-PDE, based on which the control design will be conducted next.

The control task is to design an output-feedback event-triggered control law to exponentially regulate the overall ODE-PDE-PDE system, only using the available actuation signal and boundary measurement.

3. Observer design

Considering that the actuation signals, including the ODE actuator and its delayed signal, can always be accessible in practice, we design an observer to estimate only the PDE state $u(x,t)$, i.e., the distributed state in the plant, which cannot usually be fully measured in practice but is required in the controller. Using the boundary measurement $u_x(0,t)$, the observer is built as

$$\hat{u}_t(x,t) = \varepsilon \hat{u}_{xx}(x,t) + \lambda \hat{u}(x,t) + p_1(x)(u_x(0,t) - \hat{u}_x(0,t)), \tag{13}$$
$$\hat{u}(0,t) = 0, \tag{14}$$
$$\hat{u}(1,t) = v(1,t), \tag{15}$$

where the function $p_1(x)$ is the observer gain to be determined. Defining the observer error $\tilde{u}(x,t)$ as

$$\tilde{u}(x,t) = u(x,t) - \hat{u}(x,t), \tag{16}$$

one obtains the observer error system as

$$\tilde{u}_t(x,t) = \varepsilon \tilde{u}_{xx}(x,t) + \lambda \tilde{u}(x,t) - p_1(x)\tilde{u}_x(0,t), \tag{17}$$
$$\tilde{u}(0,t) = 0, \tag{18}$$
$$\tilde{u}(1,t) = 0. \tag{19}$$

Subject to the invertible transformation

$$\tilde{u}(x,t) = \tilde{w}(x,t) - \int_0^x \alpha(x,y)\tilde{w}(y,t)dy \tag{20}$$

where

$$\alpha(x,y) = -\frac{\lambda}{\varepsilon}(1-x)\frac{I_1(\sqrt{\lambda(2-x-y)(x-y)/\varepsilon})}{\sqrt{\lambda(2-x-y)(x-y)/\varepsilon}} \tag{21}$$

for $0 \le y \le x \le 1$ with I_1 being the modified Bessel function of the first kind, the observer error system (17)–(19) with the gain $p_1(x)$ chosen as

$$p_1(x) = -\varepsilon\alpha(x,0) = \lambda(1-x)\frac{I_1(\sqrt{\lambda x(2-x)/\varepsilon})}{\sqrt{\lambda x(2-x)/\varepsilon}} \tag{22}$$

can be transformed into an exponentially stable system

$$\tilde{w}_t(x,t) = \varepsilon \tilde{w}_{xx}(x,t), \tag{23}$$
$$\tilde{w}(0,t) = 0, \tag{24}$$
$$\tilde{w}(1,t) = 0. \tag{25}$$

The inverse transformation of (20) is given in the form

$$\tilde{w}(x,t) = \tilde{u}(x,t) + \int_0^x \alpha^I(x,y)\tilde{u}(y,t)dy, \tag{26}$$

where

$$\alpha^I(x,y) = -\frac{\lambda}{\varepsilon}(1-x)\frac{J_1(\sqrt{\lambda(2-x-y)(x-y)/\varepsilon})}{\sqrt{\lambda(2-x-y)(x-y)/\varepsilon}} \tag{27}$$

with J_1 being the Bessel function of the first kind. It is straightforward to obtain from (23)–(25) that $\|\tilde{w}[t]\|^2 + \|\tilde{w}_x[t]\|^2$ is exponentially convergent to zero. According to the invertibility of backstepping transformation (20), we can easily derive the exponential stability of the observer errors in the sense of $\|\tilde{u}[t]\|^2 + \|\tilde{u}_x[t]\|^2$.

4. Continuous-in-time control design

In the last section, we have established the observer that recovers the PDE system (7)–(9) in the sense that the observer errors, in terms of the norm $\|\tilde{u}[t]\|^2 + \|\tilde{u}_x[t]\|^2$, exponentially converge to zero. In this section, we design a continuous-in-time output-feedback control law $U_f(t)$. We conduct the control design based on the observer (13)–(15) and the known part (10)–(12) of the plant, using the backstepping method, which makes the resulting control law employ only the observer states and the known signals.

Consider the invertible backstepping transformations

$$\hat{w}(x,t) = \hat{u}(x,t) - \int_0^x k(x,y)\hat{u}(y,t)\mathrm{d}y, \quad x \in [0,1] \tag{28}$$
$$z(x,t) = v(x,t) - \int_1^x p(x-y)v(y,t)\mathrm{d}y$$

$$-\int_0^1 \gamma(x,y)\hat{u}(y,t)\mathrm{d}y, \quad x\in[1,1+D] \tag{29}$$

$$y_i(t)=x_i(t)-\Gamma_{i-1}(t), \quad i\le n, i\in\mathbb{N}^* \tag{30}$$

where $k(x,y)$, $\gamma(x,y)$ and $p(s)$ are the gain kernels given by

$$k(x,y)=-\frac{\lambda}{\varepsilon}y\frac{I_1\left(\sqrt{\lambda\left(x^2-y^2\right)/\varepsilon}\right)}{\sqrt{\lambda\left(x^2-y^2\right)/\varepsilon}}, \tag{31}$$

$$\begin{aligned}\gamma(x,y)=&-2\sum_{n=1}^{\infty}\mathrm{e}^{\left(\lambda-\varepsilon\pi^2n^2\right)(x-1)}\sin(\pi ny)\\&\times\int_0^1\sin(\pi n\xi)\frac{\lambda}{\varepsilon}\xi\frac{I_1\left(\sqrt{\lambda\left(1-\xi^2\right)/\varepsilon}\right)}{\sqrt{\lambda\left(1-\xi^2\right)/\varepsilon}}\mathrm{d}\xi,\end{aligned} \tag{32}$$

$$p(s)=-\varepsilon\gamma_y(1+s,1), \quad s\in[0,D], \tag{33}$$

and where $\Gamma_i(i\le n-1, i\in\mathbb{N})$ are given by

$$\begin{aligned}\Gamma_0(t)=&\int_1^{1+D}p(1+D-y)v(y,t)dy\\&+\int_0^1\gamma(1+D,y)\hat{u}(y,t)dy,\end{aligned} \tag{34}$$

$$\begin{aligned}\Gamma_i(t)=&(-a_{i,i}-\bar{c}_i)x_i(t)+M_i^T\underline{x}_i(t)+\int_0^1 n_{i,1}(y)\hat{u}(y,t)dy\\&+\int_1^{1+D}n_{i,2}(y)v(y,t)dy, \quad i\le n-1, i\in\mathbb{N}^*\end{aligned} \tag{35}$$

with the design parameters $\bar{c}_i$ to be chosen later. The kernel functions $n_{i,1}(y)$, $n_{i,2}(y)$ and the i-dimensional vector M_i^T are recursively defined, with the bases:

$$n_{1,1}(y)=\bar{c}_1\gamma(1+D,y)+\gamma_x(1+D,y), \tag{36}$$

$$n_{1,2}(y)=\bar{c}_1p(1+D-y)+p'(1+D-y), \tag{37}$$

$$M_1^T=[p(0)], \tag{38}$$

and recursive formulas:

$$n_{i+1,1}(y)=(\bar{c}_{i+1}+\lambda)n_{i,1}(y)+\varepsilon n_{i,1}''(y), \tag{39}$$

$$n_{i+1,2}(y)=\bar{c}_{i+1}n_{i,2}(y)+n_{i,2}'(y), \tag{40}$$

$$\begin{aligned}M_{i+1}^T=&[\bar{c}_{i+1}M_i^T+M_i^TA_i, m_{i,i}-a_{i,i}-\bar{c}_i]+n_{i,2}(1+D)e_{1,i+1}^T\\&-[a_{i+1,1}, a_{i+1,2}, \ldots, a_{i+1,i}+(a_{i,i}+\bar{c}_{i+1})(a_{i,i}+\bar{c}_i), 0],\end{aligned} \tag{41}$$

for $i\le n-1, i\in\mathbb{N}^*$, where $m_{i,i}$ means the ith entry in M_i and A_i are given in (5). The detailed calculations regarding (28)–(41) are shown in Appendix A.

Lemma 1. *Applying the backstepping transformations (28)–(30) into the system consisting of (10)–(12) and (13)–(15), choosing the control law in (12) as $U_f(t)$ defined as*

$$\begin{aligned}U_f(t)=&(-a_{n,n}-\bar{c}_n)x_n(t)+\int_0^1 n_{n,1}(y)\hat{u}(y,t)dy\\&+\int_1^{1+D}n_{n,2}(y)v(y,t)dy+M_n^TX(t),\end{aligned} \tag{42}$$

we arrive at the following target system:

$$\hat{w}_t(x,t)=\varepsilon\hat{w}_{xx}(x,t)+g_1(x)\tilde{w}_x(0,t), \tag{43}$$

$$\hat{w}(0,t)=0, \tag{44}$$

$$\hat{w}(1,t)=z(1,t), \tag{45}$$

$$z_t(x,t)=z_x(x,t)+g_2(x)\tilde{w}_x(0,t), \quad x\in(1,1+D) \tag{46}$$

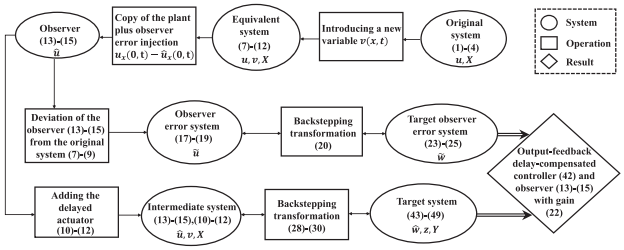

Fig. 1. Flow diagram of the observer-based delay-compensated control design.

$$z(1+D,t)=y_1(t), \tag{47}$$

$$\begin{aligned}\dot{y}_i(t)=&-\bar{c}_iy_i(t)+y_{i+1}(t)-\tilde{w}_x(0,t)\int_0^1 n_{i-1,1}(y)p_1(y)dy,\\&i\le n-1, i\in\mathbb{N}^*\end{aligned} \tag{48}$$

$$\dot{y}_n(t)=-\bar{c}_ny_n(t)-\tilde{w}_x(0,t)\int_0^1 n_{n-1,1}(y)p_1(y)dy, \tag{49}$$

where

$$n_{0,1}(y)=\gamma(1+D,y)$$

and $n_{i,1}$ for $i\le n-1, i\in\mathbb{N}^*$ are given by (36), (39), and where

$$g_1(x)=p_1(x)-\int_0^x k(x,y)p_1(y)dy, \tag{50}$$

$$g_2(x)=-\int_0^1\gamma(x,y)p_1(y)dy. \tag{51}$$

Proof. The calculation details are shown in Appendix A. □

We now complete the observer-based output-feedback delay-compensated control design, whose flow diagram is shown in Fig. 1. In summary, we represent the delay as a transport PDE and then rewrite the original system (1)–(4) as an equivalent system (7)–(12). By the boundary measurement $u_x(0,t)$, we design the observer (13)–(15) as a copy of the plant plus observer error injections that are associated with to be determined observer gain. As a result, the observer error system is (17)–(19), which is then converted into an exponentially stable system (23)–(25) by applying the backstepping transformation (20), where the observer gain $p_1(x)$ is thus determined. Applying the backstepping transformations (28)–(30) into the observer (13)–(15) and the known part (10)–(12), we arrive at the target system (43)–(49) with deriving the output-feedback delay-compensated control law as (42) where all signals come from the observer or available measurements.

Theorem 1. *For all initial conditions $X(0)\in\mathbb{R}^n$, $u[0],\hat{u}[0]\in L^2(0,1)$, $v[0]\in H^1([1,1+D])$, considering the closed-loop system that consists of the plant (7)–(12), the observer (13)–(15), and the continuous-in-time control law (42), the exponential regulation is achieved in the sense that $\Omega_1(t)$ is exponentially convergent to zero, where*

$$\Omega_1(t)=\|u[t]\|^2+\|\hat{u}[t]\|^2+\|v[t]\|^2+\|v_x[t]\|^2+|X(t)|^2. \tag{52}$$

Proof. Introduce the change of variable

$$\varpi(x,t)=\hat{w}(x,t)-xz(1,t), \tag{53}$$

we rewrite the target system under the continuous-in-time control $U_f(t)$, i.e., the system (43)–(49) into the following system:

$$\varpi_t(x,t)=\varepsilon\varpi_{xx}(x,t)-xz_t(1,t)+g_1(x)\tilde{w}_x(0,t), \tag{54}$$

$$\varpi(0,t)=0, \tag{55}$$
$$\varpi(1,t)=0, \tag{56}$$
$$z_t(x,t)=z_x(x,t)+g_2(x)\tilde{w}_x(0,t),\quad x\in(1,1+D) \tag{57}$$
$$z(1+D,t)=y_1(t), \tag{58}$$
$$\dot{y}_i(t)=-\bar{c}_i y_i(t)+y_{i+1}(t)-\tilde{w}_x(0,t)\int_0^1 n_{i-1,1}(y)p_1(y)dy,\quad i\le n-1,\ i\in\mathbb{N}^* \tag{59}$$
$$\dot{y}_n(t)=-\bar{c}_n y_n(t)-\tilde{w}_x(0,t)\int_0^1 n_{n-1,1}(y)p_1(y)dy. \tag{60}$$

We will conduct the stability analysis on the basis of the system (54)–(60), and trace to the original plant via the inverse transformation $(\varpi,z,y_i)\mapsto(\hat{u},v,x_i)$, which can be obtained as

$$\hat{u}(x,t)=\varpi(x,t)+xz(1,t)+\int_0^x l(x,y)\varpi(y,t)dy+z(1,t)\int_0^x yl(x,y)dy, \tag{61}$$
$$v(x,t)=z(x,t)+\int_1^x q(x-y)z(y,t)dy+\int_0^1\gamma^I(x,y)\varpi(y,t)dy+z(1,t)\int_0^1 y\gamma^I(x,y)dy, \tag{62}$$
$$x_i(t)=y_i(t)+\Gamma_{i-1}(t)\quad i\le n, i\in\mathbb{N}^* \tag{63}$$

by recalling (30), (53), and using the inverse transformation $(\hat{w},z)\mapsto(\hat{u},v)$ that is in the form of

$$\hat{u}(x,t)=\hat{w}(x,t)+\int_0^x l(x,y)\hat{w}(y,t)\mathrm{d}y,\quad x\in[0,1] \tag{64}$$
$$v(x,t)=z(x,t)+\int_1^x q(x-y)z(y,t)\mathrm{d}y+\int_0^1\gamma^I(x,y)\hat{w}(y,t)\mathrm{d}y,\quad x\in[1,1+D], \tag{65}$$

where

$$l(x,y)=-\frac{\lambda}{\varepsilon}y\frac{J_1\left(\sqrt{\lambda\left(x^2-y^2\right)/\varepsilon}\right)}{\sqrt{\lambda\left(x^2-y^2\right)/\varepsilon}}, \tag{66}$$
$$\gamma^I(x,y)=-2\sum_{n=1}^{\infty}\mathrm{e}^{-\varepsilon\pi^2n^2(x-1)}\sin(\pi ny)\times\int_0^1\sin(\pi n\xi)\frac{\lambda}{\varepsilon}\xi\frac{J_1\left(\sqrt{\lambda\left(1-\xi^2\right)/\varepsilon}\right)}{\sqrt{\lambda\left(1-\xi^2\right)/\varepsilon}}\mathrm{d}\xi,$$
$$q(s)=-\varepsilon\gamma_y^I(1+s,1),\quad s\in[0,D]. \tag{67}$$

We prove some inequalities that will be used in the stability analysis in the following lemma.

Lemma 2. *The following is true:*

(1) Considering the system (54)–(60), for some positive constant δ_0 to be chosen later, we have

$$\frac{d}{dt}\frac{1}{2}\|\varpi[t]\|^2\le-\left(\frac{\pi^2\varepsilon}{4}-\frac{3}{\delta_0}\right)\|\varpi[t]\|^2+\frac{\delta_0}{12}z_x^2(1,t)+\left(\frac{\delta_0}{12}g_2^2(1)+\int_0^1\frac{\delta_0}{4}g_2^2(x)dx\right)\tilde{w}_x^2(0,t). \tag{68}$$

(2) For $\tilde{w}(x,t)$ subject to (23)–(25), we obtain

$$\frac{d}{dt}\frac{1}{2}\|\tilde{w}[t]\|^2=-\varepsilon\|\tilde{w}_x[t]\|^2\le-\frac{\pi^2\varepsilon}{4}\|\tilde{w}[t]\|^2, \tag{69}$$
$$\frac{d}{dt}\frac{1}{2}\|\tilde{w}_x[t]\|^2=-\varepsilon\|\tilde{w}_{xx}[t]\|^2, \tag{70}$$
$$\tilde{w}_x^2(0,t)\le2\|\tilde{w}_x[t]\|^2+\|\tilde{w}_{xx}[t]\|^2. \tag{71}$$

(3) Considering (57)–(58), for some positive constants c_1,c_2 to be chosen later, we have

$$\begin{aligned}&\frac{d}{dt}\int_1^{1+D}e^{c_1(x-1)}z_x^2(x,t)dx\\&\le-z_x^2(1,t)+2e^{c_1D}\dot{y}_1^2(t)+2e^{c_1D}g_2^2(1+D)\tilde{w}_x^2(0,t)\\&\quad-(c_1-1)\int_1^{1+D}e^{c_1(x-1)}z_x^2(x,t)dx\\&\quad+\tilde{w}_x^2(0,t)\int_1^{1+D}e^{2c_1(x-1)}g_2'^2(x)dx,\end{aligned} \tag{72}$$
$$\begin{aligned}&\frac{d}{dt}\int_1^{1+D}e^{c_2(x-1)}z^2(x,t)dx\\&\le e^{c_2D}y_1^2(t)-z^2(1,t)-(c_2-1)\int_1^{1+D}e^{c_2(x-1)}z^2(x,t)dx\\&\quad+\tilde{w}_x^2(0,t)\int_1^{1+D}e^{2c_2(x-1)}g_2^2(x)dx.\end{aligned} \tag{73}$$

(4) Considering the inverse transformation (61)–(63), there exist positive constants q_1, q_2, q_3 and positive constant ζ related to parameters $a_{i,i}$, $\bar{c}_i$ such that

$$\|\hat{u}[t]\|^2\le q_1(\|\varpi[t]\|^2+z^2(1,t)), \tag{74}$$
$$\|v[t]\|^2\le q_2(\|z[t]\|^2+z^2(1,t)+\|\varpi[t]\|^2), \tag{75}$$
$$\|v_x[t]\|^2\le q_3(\|z[t]\|^2+\|z_x[t]\|^2+z^2(1,t)+\|\varpi[t]\|^2), \tag{76}$$
$$|X(t)|^2\le\zeta(|Y(t)|^2+\|z[t]\|^2+z^2(1,t)+\|\varpi[t]\|^2). \tag{77}$$

Proof. See Appendix B for detailed proofs. □

Before showing the Lyapunov stability of the overall system, we first conduct the Lyapunov analysis for the actuator ODE in the target system.

Applying Young's inequality into (59) we obtain

$$\dot{y}_1(t)^2\le3\bar{c}_1^2y_1(t)^2+3y_2(t)^2+q_0\tilde{w}_x(0,t)^2, \tag{78}$$

where $q_0=3(\int_0^1\gamma(1+D,y)p_1(y)dy)^2$. Next, using (59) and (60), we take the time derivative of $y_i(t)^2$:

$$\frac{d}{dt}y_i(t)^2\le-2(\bar{c}_i-1)y_i(t)^2+y_{i+1}(t)^2+g_{3i}\tilde{w}_x(0,t)^2 \tag{79}$$

for $i\le n-1$, $i\in\mathbb{N}^*$, and

$$\frac{d}{dt}y_n(t)^2\le-2(\bar{c}_n-\frac{1}{2})y_n(t)^2+g_{3n}\tilde{w}_x(0,t)^2 \tag{80}$$

where $g_{3i}=(\int_0^1 n_{i-1,1}p_1(y)dy)^2$ for $i\le n$, $i\in\mathbb{N}^*$. From (79) and (80) we have

$$\frac{d}{dt}|Y(t)|^2\le-2(\bar{c}_1-1)y_1(t)^2-2(\bar{c}_n-1)y_n(t)^2+\sum_{i=1}^{n}g_{3i}\tilde{w}_x(0,t)^2-\sum_{i=2}^{n-1}2(\bar{c}_i-\frac{3}{2})y_i(t)^2. \tag{81}$$

Define a Lyapunov function as

$$\begin{aligned}V_1(t)=&\frac{1}{2}\int_0^1\varpi^2(x,t)dx+3r_{1a}\int_0^1\tilde{w}^2(x,t)dx\\&+r_{1b}\int_1^{1+D}\mathrm{e}^{c_1(x-1)}z_x^2(x,t)dx+\frac{r_{1c}}{2}\int_0^1\tilde{w}_x^2(x,t)dx\\&+\int_1^{1+D}\mathrm{e}^{c_2(x-1)}z^2(x,t)dx+r_{1e}|Y(t)|^2\end{aligned} \tag{82}$$

where $r_{1a}, r_{1b}, r_{1c}, r_{1e}, c_1, c_2$ are positive constants to be chosen later. Using (68)–(73), (78), and (81), we obtain

$$\begin{aligned}\dot{V}_1 \leq & -(\frac{\pi^2\varepsilon}{4}-\frac{3}{\delta_0})\|\varpi[t]\|^2-(r_{1b}-\frac{\delta_0}{12})z_x^2(1,t)\\ & -r_{1a}\pi^2\varepsilon\|\tilde{w}[t]\|^2-(2r_{1a}\varepsilon-2F_1)\|\tilde{w}_x[t]\|^2\\ & -r_{1b}(c_1-1)\int_1^{1+D}e^{c_1(x-1)}z_x^2(x,t)dx\\ & +2r_{1b}e^{c_1D}(3\bar{c}_1^2y_1(t)^2+3y_2(t)^2)-(r_{1c}\varepsilon-F_1)\|\tilde{w}_{xx}[t]\|^2\\ & -(c_2-1)\int_1^{1+D}e^{c_2(x-1)}z^2(x,t)dx\\ & +e^{c_2D}y_1(t)^2-z^2(1,t)-2r_{1e}(\bar{c}_1-1)y_1(t)^2\\ & -2r_{1e}\sum_{i=2}^{n-1}\left(\bar{c}_i-\frac{3}{2}\right)y_i(t)^2-2r_{1e}(\bar{c}_n-1)y_n(t)^2 \end{aligned} \tag{83}$$

where the constant F_1 is

$$\begin{aligned}F_1=&\frac{\delta_0}{12}g_2^2(1)+\int_0^1\frac{\delta_0}{4}g_1^2(x)dx+2r_{1b}e^{c_1D}g_2^2(1+D)\\ &+r_{1b}\int_1^{1+D}e^{2c_1(x-1)}g_2'^2(x)dx+2r_{1b}e^{c_1D}q_0\\ &+\int_1^{1+D}e^{2c_2(x-1)}g_2^2(x)dx+r_{1e}\sum_{i=1}^{n}g_{3i}. \end{aligned} \tag{84}$$

Choosing the following parameters to satisfy $\delta_0 > \frac{12}{\pi^2\varepsilon}$, $r_{1b} \geq \delta_0/12$, $c_1 > 1$, $c_2 > 1$, $r_{1e} > \max\left\{\frac{e^{c_2D}+6r_{1b}\bar{c}_1^2e^{c_1D}}{2(\bar{c}_1-1)}, \frac{6r_{1b}e^{c_1D}}{2(\bar{c}_2-\frac{3}{2})}\right\}$, $r_{1a} > F_1/\varepsilon$, $r_{1c} \geq F_1/\varepsilon$, and $\bar{c}_i > \frac{3}{2}$ for $i = 1, 2, \ldots, n$, we then arrive

$$\begin{aligned}\dot{V}_1 \leq & -(r_{1b}-\frac{\delta_0}{12})z_x^2(1,t)-\nu_1\|\varpi[t]\|^2-z(1,t)^2\\ & -(c_2-1)\int_1^{1+D}e^{c_2(x-1)}z^2(x,t)dx-\nu_2y_1(t)^2\\ & -\nu_3y_2(t)^2-\sum_{i=3}^{n}\nu_{4i}y_i(t)^2-r_{1a}\pi^2\varepsilon\|\tilde{w}[t]\|^2\\ & -(r_{1c}\varepsilon-F_1)\|\tilde{w}_{xx}[t]\|^2-(2r_{1a}\varepsilon-2F_1)\|\tilde{w}_x[t]\|^2\\ & -r_{1b}(c_1-1)\int_1^{1+D}e^{c_1(x-1)}z_x^2(x,t)dx\\ \leq & -\sigma_1V_1 \end{aligned} \tag{85}$$

where $\nu_1 = \frac{\pi^2\varepsilon}{4}-\frac{3}{\delta_0}$, $\nu_2 = 2r_{1e}(\bar{c}_1-1)-e^{c_2D}-6r_{1b}\bar{c}_1^2e^{c_1D}$, $\nu_3 = 2r_{1e}(\bar{c}_2-\frac{3}{2})-6r_{1b}e^{c_1D}$, $\nu_{4i} = 2r_{1e}(\bar{c}_i-\frac{3}{2})$ for $i \geq 3$ (if $n < 3$ then there is no ν_{4i}) and

$$\sigma_1 = \min\left\{2\nu_1, c_1-1, c_2-1, \frac{4r_{1a}\varepsilon-4F_1}{r_{1c}}, \frac{\nu_2}{r_{1e}}, \frac{\nu_3}{r_{1e}}, \frac{\nu_{4i}}{r_{1e}}\right\} \tag{86}$$

are positive constants. Thus we can obtain the following:

$$V_1(t) \leq e^{-\sigma_1 t}V_1(0). \tag{87}$$

Defining

$$\begin{aligned}\Upsilon_1(t)=&\|\varpi[t]\|^2+\|\tilde{w}[t]\|^2+\|\tilde{w}_x[t]\|^2+\|z_x[t]\|^2\\ &+\|z[t]\|^2+|Y(t)|^2, \end{aligned} \tag{88}$$

we have $\xi_1\Upsilon_1(t) \leq V_1(t) \leq \xi_2\Upsilon_1(t)$ where $\xi_1 = \min\{\frac{1}{2}, 3r_{1a}, r_{1b}, \frac{r_{1c}}{2}, r_{1e}\} > 0, \xi_2 = \max\left\{\frac{1}{2}, 3r_{1a}, r_{1b}e^{c_1D}, \frac{r_{1c}}{2}, e^{c_2D}, r_{1e}\right\} > 0$. Thus we get

$$\Upsilon_1(t) \leq \frac{\xi_2}{\xi_1}\Upsilon_1(0)e^{-\sigma_1 t}. \tag{89}$$

Applying the Cauchy–Schwarz inequality into (20), we can obtain

$$\|\tilde{u}[t]\|^2 \leq q_4\|\tilde{w}[t]\|^2, \tag{90}$$

where $q_4 = 2(1+\int_0^1\int_0^x\alpha(x,y)^2dydx)$. We obtain from (16) that

$$\|u[t]\|^2 \leq 2\|\tilde{u}[t]\|^2+2\|\hat{u}[t]\|^2. \tag{91}$$

With Agmon's inequality, it can be proved that

$$z^2(1,t) \leq \frac{1+D}{D}\|z[t]\|^2+\|z_x[t]\|^2. \tag{92}$$

Therefore, recalling (52), using (74)–(77) and (89)–(92), we have

$$\begin{aligned}\Omega_1(t) \leq & \left(3q_1+2q_2+2q_3+2\zeta+\frac{3q_1+q_2+q_3+\zeta}{D}\right)\|z[t]\|^2\\ & +(3q_1+q_2+2q_3+\zeta)(\|\varpi[t]\|^2+\|z_x[t]\|^2)\\ & +2q_4\|\tilde{w}[t]\|^2+\zeta|Y(t)|^2\\ \leq & \varrho_1\Upsilon_1(t) \leq \varrho_1\frac{\Upsilon_1(0)\xi_2}{\xi_1}e^{-\sigma_1 t} \end{aligned} \tag{93}$$

where $\varrho_1 = \max\{3q_1+2q_2+2q_3+2\zeta+\frac{3q_1+q_2+q_3+\zeta}{D}, 2q_4\} > 0$. It implies that $\Omega_1(t)$ is exponentially convergent to zero.

The proof of this theorem is complete. □

5. Event-triggered control design

In this section, we extend the observer-based delay-compensated controller built in the last section, to the event-triggered type, where the continuous-in-time controller $U_f(t)$ given by (42) is updated at a certain sequence of time instants $(t_j)_{j\in\mathbb{N}}$ that will be determined by an event-triggering mechanism (ETM), and the control input is held constant between two successive time instants.

We define the event-triggered control input $U_d(t)$ as

$$\begin{aligned}U_d(t) :=&U_f(t_j)\\ =&(-a_{n,n}-\bar{c}_n)x_n(t_j)+\int_0^1 n_{n,1}(y)\hat{u}(y,t_j)dy\\ &+\int_1^{1+D}n_{n,2}(y)v(y,t_j)dy+M_n^TX(t_j), \end{aligned} \tag{94}$$

for $t \in [t_j, t_{j+1}), j \in \mathbb{N}$. Define the difference between the continuous-in-time control signal $U_f(t)$ in (42) and the event-triggered control input U_d in (94) as $d(t)$, given by

$$\begin{aligned}d(t) :=&U_f(t)-U_d\\ =&-(a_{n,n}+\bar{c}_n)(x_n(t)-x_n(t_j))\\ &+\int_0^1 n_{n,1}(y)(\hat{u}(y,t)-\hat{u}(y,t_j))dy\\ &+\int_1^{1+D}n_{n,2}(y)(v(y,t)-v(y,t_j))dy\\ &+M_n^T(X(t)-X(t_j)), \end{aligned} \tag{95}$$

for $t \in [t_j, t_{j+1})$, which reflects the deviation of the plant states from their sampled values and will be used in building the ETM.

The sequence of time instants $I = \{t_0, t_1, t_2, \ldots\}$ $(t_0 = 0)$ is defined by the following ETM ($j \in \mathbb{N}$):

(a) if $\left\{t \in \mathbb{R}_+ \mid t > t_j \wedge d^2(t) > -\xi m(t)\right\} = \emptyset$, then the set of the times of the events is $\{t_0, \ldots, t_j\}$,

(b) if $\left\{t \in \mathbb{R}_+ \mid t > t_j \wedge d^2(t) > -\xi m(t)\right\} \neq \emptyset$, then the next triggering time is given by

$$t_{j+1} = \inf\left\{t > t_j : d(t)^2 \geq -\xi m(t)\right\}, \tag{96}$$

where the positive constant ξ is a design parameter and the dynamic variable $m(t)$ in (96) satisfies the ODE

$$\dot{m}(t) = -\eta m(t) + \lambda_d d(t)^2 - \kappa_1 \|v[t]\|^2 - \kappa_2 \|\hat{u}[t]\|^2 - \kappa_3 \tilde{u}_x^2(0,t) - \kappa_4 |X(t)|^2 \tag{97}$$

for $t \in (t_j, t_{j+1})$ with $m(t_0) = m(0) < 0$. The design parameter $\eta > 0$ is free and positive parameters $\lambda_d, \kappa_1, \kappa_2, \kappa_3, \kappa_4$ are to be selected to ensure the minimal dwell time under the proposed ETM (96) is larger than a positive constant, i.e., no Zeno behavior, which will be shown in Lemma 4. It is worth noting that the initial condition for $m(t)$ in each time interval has been chosen such that $m(t)$ is time-continuous. Therefore, we define $m(t_j^-) = m(t_j) = m(t_j^+)$. Inserting $d(t)^2 \le -\xi m(t)$ guaranteed by (96) into (97), we have

$$\dot{m}(t) \le -(\eta + \lambda_d \xi) m(t) - \kappa_1 \|v[t]\|^2 - \kappa_2 \|\hat{u}[t]\|^2 - \kappa_3 \tilde{u}_x^2(0,t) - \kappa_4 |X(t)|^2 \tag{98}$$

for $t \in (t_j, t_{j+1})$. Considering the time continuity of $m(t)$, we can obtain from (98) that

$$m(t) \le m(t_j) e^{-(\eta+\lambda_d\xi)(t-t_j)} - \int_{t_j}^{t} e^{-(\eta+\lambda_d\xi)(t-\varepsilon)} \left(\kappa_1 \|v[\varepsilon]\|^2 + \kappa_2 \|\hat{u}[\varepsilon]\|^2 + \kappa_3 \tilde{u}_x^2(0,\varepsilon) + \kappa_4 |X(\varepsilon)|^2\right) d\varepsilon \tag{99}$$

for $t \in [t_j, t_{j+1}]$, $j \in \mathbb{N}$. We choose $m(0) < 0$ such that both terms on the right-hand side of (99) are less than zero for $t \in [0, t_1]$. It is easily derived that $m(t) < 0$ for $t \in [0, t_1]$. Again by using $m(t_1) < 0$ we obtain $m(t) < 0$ for $t \in [t_1, t_2]$. By recursion, we derive $m(t) < 0$ all the time.

To discuss the well-posedness issue of this event-based closed-loop system with delayed actuation, we define a new increasing sequence of times $\{\tau_i \ge 0, i = 0, 1, 2, \ldots\}$ as

$$\tau_0 = t_0, \ \ \tau_i = t_i + D, \ \ i \in \mathbb{N}^*. \tag{100}$$

We have the following proposition regarding the well-posedness issue.

Proposition 1. *For $X(\tau_i) \in \mathbb{R}^n$, $u[\tau_i], \hat{u}[\tau_i] \in L^2(0,1)$, $v[\tau_i] \in C^{n-1}([1, 1+D])$ with $v[\tau_i] \in C^n([1, 1+D]\backslash I_{\tau_i})$ where $I_{\tau_i} = \{x^j_{\tau_i} | x^j_{\tau_i} = 1+(\tau_{i+j}-\tau_i)$ and $x^j_{\tau_i} \le 1+D, j \in \mathbb{N}\}$ is a set of finitely many points on $[1, 1+D]$, there exist unique mappings $u, \hat{u} \in C^0([\tau_i, \tau_{i+1}]; L^2(0,1))$ with $u, \hat{u} \in C^1((\tau_i, \tau_{i+1}) \times [0,1])$ satisfying $u[t], \hat{u}[t] \in C^2([0,1])$ for all $t \in (\tau_i, \tau_{i+1}]$, $v \in C^1([\tau_i, \tau_{i+1}] \times [1, 1+D])$ with $v \in C^2([\tau_i, \tau_{i+1}] \times [1, 1+D] \setminus L_{\tau_i})$ where L_{τ_i} denotes the isolated curves in the rectangle $[\tau_i, \tau_{i+1}] \times [1, 1+D]$, and $X \in C^0([\tau_i, \tau_{i+1}], \mathbb{R}^n)$ to the system (7)–(12) with the control input (94).*

Proof. For $t \in [\tau_i, \tau_{i+1})$, timing $e^{A_n t}$ into both sides of (12), and integrating from τ_i to t, we directly obtain a (weak) solution belonging to $C^0([\tau_i, \tau_{i+1}]; \mathbb{R}^n)$ as $X(t) = X(\tau_i)e^{-A_n t} + \int_{\tau_i}^{t} e^{A_n(\tau-t)} e_{n,n} U(\tau) d\tau$ where $U(t)$ is piecewise-constant on $t \in [\tau_i, \tau_{i+1})$. Recalling A_n, $e_{n,n}$ defined by (5) and (6), together with $n > 1$, we have that $x_1(t) \in C^1([\tau_i, \tau_{i+1}], \mathbb{R})$. Applying Corollary 2.3 in Karafyllis and Krstic (2019), it follows from $x_1(t) \in C^1([\tau_i, \tau_{i+1}], \mathbb{R})$ and $v[\tau_i] \in C^{n-1}([1, 1+D])$ with $v[\tau_i] \in C^n([1, 1+D] \setminus I_{\tau_i})$ $(n > 1)$ that there exists a unique mapping $v[t] \in C^1([\tau_i, \tau_{i+1}] \times [1, 1+D])$ with $v \in C^2([\tau_i, \tau_{i+1}] \times [1, 1+D] \setminus L_{\tau_i})$ satisfying (10), (11). Because of $v(1,t) \in C^1([\tau_i, \tau_{i+1}])$ with $v(1,t) \in C^2((\tau_i, \tau_{i+1}))$ and $u[\tau_i] \in L^2(0,1)$, applying Theorem 4.11 in Karafyllis and Krstic (2019), there exists a unique mapping $u \in C^0([\tau_i, \tau_{i+1}]; L^2(0,1))$ with $u \in C^1((\tau_i, \tau_{i+1}) \times [0,1])$ satisfying $u[t] \in C^2([0,1])$ for all $t \in (\tau_i, \tau_{i+1}]$ to (7)–(9).

It follows from $u[\tau_i], \hat{u}[\tau_i] \in L^2(0,1)$ and (16) that $\tilde{u}[\tau_i] \in L^2(0,1)$. Considering (26), it means that $\tilde{w}[\tau_i] \in L^2(0,1)$. Applying Theorem 4.1 in Karafyllis and Krstic (2019), there exists a unique mapping $\tilde{w} \in C^0([\tau_i, \tau_{i+1}]; L^2(0,1))$ with $\tilde{w} \in C^1((\tau_i, \tau_{i+1}] \times [0,1])$ satisfying $\tilde{w}[t] \in C^2([0,1])$ for all $t \in (\tau_i, \tau_{i+1}]$. Recalling the transformation (20), we have that there exists a unique mapping $\tilde{u} \in C^0([\tau_i, \tau_{i+1}]; L^2(0,1))$ with $\tilde{u} \in C^1((\tau_i, \tau_{i+1}] \times [0,1])$ satisfying $\tilde{u}[t] \in C^2([0,1])$ for all $t \in (\tau_i, \tau_{i+1}]$. According to the solutions $u, \tilde{u}$ obtained above, recalling (16), we have that there exists a unique mapping $\hat{u} \in C^0([\tau_i, \tau_{i+1}]; L^2(0,1))$ with $\hat{u} \in C^1((\tau_i, \tau_{i+1}) \times [0,1])$ satisfying $\hat{u}[t] \in C^2([0,1])$ for all $t \in (\tau_i, \tau_{i+1}]$. □

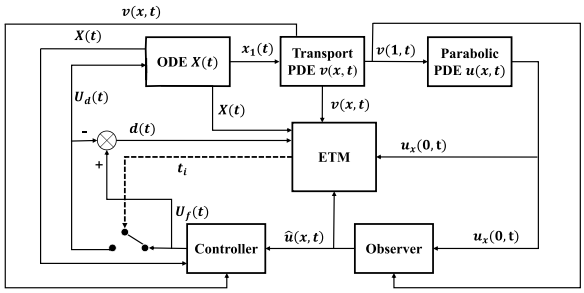

Fig. 2. Block diagram of the event-based closed-loop system.

6. Main results

The block diagram of the closed-loop system consisting of the plant, observer, controller, and event-triggering mechanism is presented in Fig. 2. The main results of the event trigger design are shown as follows.

Theorem 2. *For all initial conditions $X(0) \in \mathbb{R}^n$, $u[0], \hat{u}[0] \in L^2(0,1)$, $v[0] \in C^n([1, 1+D])$, and $m(0) \in \mathbb{R}_-$, the closed-loop system, which consists of the plant (7)–(12), the observer (13)–(15) and the event-triggered control law $U_d(t)$ (94) with the event-triggering mechanism (96), (97), has the following properties:*

(1) There exists a unique solution $u, \hat{u} \in C^0(\mathbb{R}^+; L^2(0,1))$ with $u, \hat{u} \in C^1(J \times [0,1])$ satisfying $u[t], \hat{u}[t] \in C^2([0,1])$ for all $t \in (0, \infty)$, where $J = \mathbb{R}^+ \setminus \{\tau_i \ge 0, i \in \mathbb{N}\}$ with τ_i defined by (100), and $v \in C^1(\mathbb{R}^+ \times [1, 1+D])$ as well as $X \in \mathbb{C}^0(\mathbb{R}^+, \mathbb{R}^n)$.

(2) The exponential regulation is archived in the sense that $\Omega(t)$ and $U_d(t)$ exponentially converge to zero, where

$$\Omega(t) = \|u[t]\|^2 + \|\hat{u}[t]\|^2 + \|v[t]\|^2 + \|v_x[t]\|^2 + |X(t)|^2 + |m(t)|. \tag{101}$$

Proof. The detailed process is shown next. □

6.1. Proof of well-posedness

First, we show the proof of no Zeno phenomenon through the following two lemmas.

Lemma 3. *For $d(t)$ defined in (95), there exist positive constants $\epsilon_1, \epsilon_2, \epsilon_3, \epsilon_4, \epsilon_5$ such that*

$$\dot{d}(t)^2 \le \epsilon_1 d(t)^2 + \epsilon_2 \|v[t]\|^2 + \epsilon_3 \|\hat{u}[t]\|^2 + \epsilon_4 \tilde{u}_x^2(0,t) + \epsilon_5 |X(t)|^2 \tag{102}$$

for $t \in (t_j, t_{j+1})$.

Proof. The event-triggered control input U_d is constant on $t \in (t_j, t_{j+1})$, i.e., $\dot{U}_d(t) = 0$. Taking the time derivative of (95),

recalling (7)–(12), (32), (33), (42), and (94), applying integration by parts, we obtain that

$$\begin{aligned}\dot{d}(t) =&(-a_{n,n}-\bar{c}_n)\dot{x}_n(t)+\int_0^1 n_{n,1}(y)\hat{u}_t(y,t)dy\\ &+\int_1^{1+D} n_{n,2}(y)v_t(y,t)dy+M_n^T\dot{X}(t)\\ =&b_1 d(t)+B_2X(t)+\int_0^1 b_3(y)\hat{u}(y,t)dy\\ &+\int_1^{1+D} b_4(y)v(y,t)dy+b_5\tilde{u}_x(0,t)\end{aligned} \tag{103}$$

for $t\in(t_j,t_{j+1})$, where

$$b_1 = a_{n,n}+\bar{c}_n-m_{n,n}, \tag{104}$$

$$B_2 = M_n^TA_n-b_1M_n^T+b_1(a_{n,n}+\bar{c}_n)e_{n,n}^T+n_{n,2}(1+D)e_{1,n}^T, \tag{105}$$

$$b_3(y) = \varepsilon n_{n,1}''(y)+(\lambda-b_1)n_{n,1}(y), \tag{106}$$

$$b_4(y) = n_{n,2}'(y)-b_1n_{n,2}(y), \tag{107}$$

$$b_5 = \int_0^1 n_{n,1}(y)p_1(y)dy. \tag{108}$$

Applying the Cauchy–Schwarz inequality into (103), we then obtain (102), where

$$\epsilon_1 = 5b_1^2,\ \epsilon_2 = 5\int_1^{1+D} b_4(y)^2dy,$$

$$\epsilon_3 = 5\int_0^1 b_3(y)^2dy,\ \epsilon_4 = 5b_5^2,\ \epsilon_5 = 5|B_2|^2.\quad\square \tag{109}$$

Lemma 4. *Under the event-triggered delay-compensated boundary controller defined in (94), for some positive $\kappa_1,\kappa_2,\kappa_3,\kappa_4$ in (97), there exists a minimal dwell-time $\tau>0$ such that $t_{j+1}-t_j>\tau$ for all $j\in\mathbb{N}$, which is independent of the initial conditions.*

Proof. Inspired by Espitia (2020), we introduce the following auxiliary function $\psi(t)$:

$$\psi(t) = \frac{d(t)^2+\frac{1}{2}\xi m(t)}{-\frac{1}{2}\xi m(t)} \tag{110}$$

to show the avoidance of the Zeno phenomenon.

In (110), we have that $\psi\left(t_{j+1}^-\right)=1$ because $d^2(t_{j+1}^-)=-\xi m(t_{j+1})$, and that $\psi\left(t_j\right)<0$ because $d\left(t_j\right)=0$ according to (95). The function $\psi(t)$ is a continuous function on $\left[t_j,t_{j+1}^-\right]$ recalling (95) and $\hat{u}\in C^0\left(\left[t_j,t_{j+1}\right];L^2(0,1)\right)$, $v\in C^0\left(\left[t_j,t_{j+1}\right];L^2(1,1+D)\right)$,

$X\in C^0\left(\left[t_j,t_{j+1}\right];\mathbb{R}^n\right)$, $m\in C^0\left(\left[t_j,t_{j+1}\right];\mathbb{R}_-\right)$. By the intermediate value theorem, there exists a $t^*\in\left(t_j,t_{j+1}\right)$ such that $\psi(t)\in[0,1]$ when $t\in\left[t^*,t_{j+1}^-\right]$. The minimal dwell time can be found as the minimal time it takes for $\psi(t)$ from 0 to 1. Taking the time derivative of (110), one obtains

$$\begin{aligned}\dot{\psi} =&\frac{2d(t)\dot{d}(t)+\frac{1}{2}\xi\dot{m}(t)}{-\frac{1}{2}\xi m(t)}-\frac{\dot{m}(t)}{m(t)}\psi(t)\\ \le&\frac{1}{-\frac{1}{2}\xi m(t)}\Big(\epsilon_1 d(t)^2+\epsilon_2\|v[t]\|^2+\epsilon_3\|\hat{u}[t]\|^2+\epsilon_4\tilde{u}_x^2(0,t)\\ &+\epsilon_5|X(t)|^2+d(t)^2-\frac{1}{2}\xi\eta m(t)+\frac{1}{2}\xi\lambda_d d(t)^2\\ &-\frac{1}{2}\xi\kappa_1\|v[t]\|^2-\frac{1}{2}\xi\kappa_2\|\hat{u}[t]\|^2-\frac{1}{2}\xi\kappa_3\tilde{u}_x^2(0,t)\\ &-\frac{1}{2}\xi\kappa_4|X(t)|^2\Big)-\frac{\lambda_d d(t)^2}{m(t)}\psi(t)+\eta\psi(t)\\ =&-\frac{-\kappa_1\|v[t]\|^2-\kappa_2\|\hat{u}[t]\|^2-\kappa_3\tilde{u}_x^2(0,t)-\kappa_4|X(t)|^2}{m(t)}\psi.\end{aligned} \tag{111}$$

Note that the last term in (111) is less than zero. Choosing the design parameters $\kappa_1,\kappa_2,\kappa_3,\kappa_4$ as

$$\kappa_1\ge\frac{2\epsilon_2}{\xi},\kappa_2\ge\frac{2\epsilon_3}{\xi},\kappa_3\ge\frac{2\epsilon_4}{\xi},\kappa_4\ge\frac{2\epsilon_5}{\xi} \tag{112}$$

where $\epsilon_2,\epsilon_3,\epsilon_4,\epsilon_5$ are given in (109), then (111) becomes

$$\begin{aligned}\dot{\psi}\le&\frac{1}{-\frac{1}{2}\xi m(t)}\left(\left(\epsilon_1+1+\frac{1}{2}\xi\lambda_d\right)d(t)^2-\frac{1}{2}\xi\eta m(t)\right)\\ &-\frac{\lambda_d d(t)^2}{m(t)}\psi+\eta\psi.\end{aligned} \tag{113}$$

Applying $\frac{d(t)^2}{m(t)}=\frac{d(t)^2+\frac{1}{2}\xi m(t)-\frac{1}{2}\xi m(t)}{m(t)}=-\frac{1}{2}\xi(\psi(t)+1)$, we obtain from (113) that

$$\dot{\psi}\le\bar{n}_1\psi^2+\bar{n}_2\psi+\bar{n}_3 \tag{114}$$

where $\bar{n}_1=\frac{1}{2}\lambda_d\xi$, $\bar{n}_2=1+\epsilon_1+\lambda_d\xi+\eta$, $\bar{n}_3=1+\eta+\epsilon_1+\frac{1}{2}\lambda_d\xi$ are positive constants. By the comparison principle, it follows that the time interval $t_{j+1}-t^*\ge\tau$ where

$$\tau=\int_0^1\frac{1}{\bar{n}_3+\bar{n}_2s+\bar{n}_1s^2}ds>0. \tag{115}$$

As $t_{j+1}-t_j>t_{j+1}-t^*$, we can conclude that $t_{j+1}-t_j>\tau$. Note that τ is independent of initial conditions. $\square$

Lemma 4 implies that $\lim_{i\to\infty}t_i=+\infty$, i.e., $\lim_{i\to\infty}\tau_i=+\infty$ recalling (100). Thus, Property 1 follows as a direct consequence of Proposition 1, by repeating the construction on every interval between τ_i and τ_{i+1}.

6.2. Proof of exponential convergence

We use the change of variable (53) to rewrite the target system under the event-triggered control U_d into the system (54)–(59) cascaded with

$$\dot{y}_n(t)=-\bar{c}y_n(t)-d(t)-\tilde{w}_x(0,t)\int_0^1 n_{n-1,1}(y)p_1(y)dy. \tag{116}$$

Define a Lyapunov function in the event-based closed-loop system as

$$\begin{aligned}V(t)=&\frac{r_0}{2}\int_0^1\varpi^2(x,t)dx+3r_a\int_0^1\tilde{w}^2(x,t)dx\\ &+r_b\int_1^{1+D}e^{c_1(x-1)}z_x^2(x,t)dx+\frac{r_c}{2}\int_0^1\tilde{w}_x^2(x,t)dx\\ &+r_d\int_1^{1+D}e^{c_2(x-1)}z^2(x,t)dx+r_e|Y(t)|^2-m(t)\end{aligned} \tag{117}$$

where $m(t)$ is defined in (97) and $r_0,r_a,r_b,r_c,r_d,r_e,c_1,c_2$ are positive constants to be chosen later. In the event-based situation, (68)–(77) in Lemma 2 still hold and the inequality for the actuator ODE becomes

$$\begin{aligned}\frac{d}{dt}|Y(t)|^2\le&-2(\bar{c}_1-1)y_1(t)^2+d(t)^2+\sum_{i=1}^n g_{3i}\tilde{w}_x(0,t)^2\\ &-\sum_{i=2}^n 2(\bar{c}_i-\frac{3}{2})y_i(t)^2.\end{aligned} \tag{118}$$

Using (68)–(73), (78), (97), and (118), we obtain

$$\dot{V}\le-r_0(\frac{\pi^2\varepsilon}{4}-\frac{3}{\delta_0})\|\varpi[t]\|^2-(r_b-\frac{\delta_0r_0}{12})z_x^2(1,t)$$

$$
\begin{aligned}
&- r_a\pi^2\varepsilon\|\tilde{w}[t]\|^2 - (2r_a\varepsilon - 2F)\|\tilde{w}_x[t]\|^2 \\
&- r_b(c_1-1)\int_1^{1+D} e^{c_1(x-1)}z_x^2(x,t)dx \\
&+ 2r_be^{c_1D}(3\bar{c}_1^2y_1(t)^2 + 3y_2(t)^2) - (r_c\varepsilon - F)\|\tilde{w}_{xx}[t]\|^2 \\
&- r_d(c_2-1)\int_1^{1+D} e^{c_2(x-1)}z^2(x,t)dx \\
&+ r_de^{c_2D}y_1(t)^2 - r_dz^2(1,t) - 2r_e(\bar{c}_1-1)y_1(t)^2 \\
&- 2r_e\sum_{i=2}^{n}\left(\bar{c}_i - \frac{3}{2}\right)y_i(t)^2 + (r_e-\lambda_d)d(t)^2 + \eta m(t) \\
&+ \kappa_1\|v[t]\|^2 + \kappa_2\|\hat{u}[t]\|^2 + \kappa_4|X(t)|^2
\end{aligned} \tag{119}
$$

for $t \in (t_j, t_{j+1})$, where the constant F is

$$
\begin{aligned}
F =& \frac{\delta_0 r_0}{12}g_2^2(1) + \int_0^1 \frac{\delta_0 r_0}{4}g_1^2(x)dx + 2r_be^{c_1D}g_2^2(1+D) \\
&+ r_b\int_1^{1+D} e^{2c_1(x-1)}g_2'^2(x)dx + 2r_be^{c_1D}q_0 \\
&+ r_d\int_1^{1+D} e^{2c_2(x-1)}g_2^2(x)dx + r_e\sum_{i=1}^{n} g_{3i} + \kappa_3.
\end{aligned} \tag{120}
$$

Choosing the following parameters to satisfy

$$\delta_0 > \frac{12}{\pi^2\varepsilon}, \tag{121}$$

$$r_0 > \frac{q_1\kappa_2 + q_2\kappa_1 + \kappa_4\zeta}{\frac{\pi^2\varepsilon}{4} - \frac{3}{\delta_0}}, \tag{122}$$

$$r_b \geq \delta_0 r_0/12,\ \ r_d \geq q_1\kappa_2 + q_2\kappa_1 + \kappa_4\zeta, \tag{123}$$

$$c_1 > 1,\ \ c_2 > 1 + \frac{q_2\kappa_1 + \kappa_4\zeta}{r_d}, \tag{124}$$

$$\bar{c}_1 > 1,\ \ \bar{c}_i > \frac{3}{2},\ \ i = 2, 3, \ldots, n, \tag{125}$$

$$
\begin{aligned}
r_e > \max\Bigg\{&\frac{r_de^{c_2D} + 6r_b\bar{c}_1^2e^{c_1D} + \kappa_4\zeta}{2(\bar{c}_1-1)}, \\
&\frac{6r_be^{c_1D} + \kappa_4\zeta}{2(\bar{c}_2 - \frac{3}{2})}, \frac{\kappa_4\zeta}{2(\bar{c}_i - \frac{3}{2})}\Bigg\},
\end{aligned} \tag{126}
$$

$$\lambda_d \geq r_e, \tag{127}$$

$$r_a > F/\varepsilon, r_c \geq F/\varepsilon, \tag{128}$$

we then arrive

$$
\begin{aligned}
\dot{V} \leq& -(r_b - \frac{\delta_0 r_0}{12})z_x^2(1,t) + \eta m(t) - \mu_1\|\varpi[t]\|^2 - \mu_2 d(t)^2 \\
&- \mu_3 z(1,t)^2 - \mu_4\int_1^{1+D} e^{c_2(x-1)}z^2(x,t)dx - \mu_5 y_1(t)^2 \\
&- \mu_6 y_2(t)^2 - \sum_{i=3}^{n}\mu_{7i}y_i(t)^2 - r_a\pi^2\varepsilon\|\tilde{w}[t]\|^2 \\
&- (r_c\varepsilon - F)\|\tilde{w}_{xx}[t]\|^2 - (2r_a\varepsilon - 2F)\|\tilde{w}_x[t]\|^2 \\
&- r_b(c_1-1)\int_1^{1+D} e^{c_1(x-1)}z_x^2(x,t)dx \\
\leq& -\sigma V
\end{aligned} \tag{129}
$$

for $t \in (t_j, t_{j+1}), j \in \mathbb{N}$, where $\mu_1 = r_0(\frac{\pi^2\varepsilon}{4} - \frac{3}{\delta_0}) - q_1\kappa_2 - q_2\kappa_1 - \kappa_4\zeta$, $\mu_2 = \lambda_d - r_e$, $\mu_3 = r_d - q_1\kappa_2 - q_2\kappa_1 - \kappa_4\zeta$, $\mu_4 = r_d(c_2 - 1) - q_2\kappa_1 - \kappa_4\zeta$, $\mu_5 = 2r_e(\bar{c}_1 - 1) - r_de^{c_2D} - 6r_b\bar{c}_1^2e^{c_1D} - \kappa_4\zeta$, $\mu_6 = 2r_e(\bar{c}_2 - \frac{3}{2}) - \kappa_4\zeta - 6r_be^{c_1D}$, $\mu_{7i} = 2r_e(\bar{c}_i - \frac{3}{2}) - \kappa_4\zeta$ for $i \geq 3$ (if $n < 3$ then there is no μ_{7i}) and

$$\sigma = \min\left\{\frac{2\mu_1}{r_0}, \frac{\mu_4}{r_d}, \frac{\pi^2\varepsilon}{3}, \frac{4r_a\varepsilon - 4F}{r_c}, \frac{\mu_5}{r_e}, \frac{\mu_6}{r_e}, \frac{\mu_{7i}}{r_e}, c_1 - 1, \eta\right\} \tag{130}$$

are positive constants.

Concentrating on this time interval, we can show that $V\left(t_{j+1}^-\right) \leq e^{-\sigma\left(t_{j+1}^- - t_j^+\right)}V\left(t_j^+\right)$. Here, t_j^+ and t_j^- are the right and left limits of $t = t_j$. Since $V(t)$ is continuous (as $\varpi(x,t)$, $\tilde{w}(x,t)$, $\tilde{w}_x(x,t)$, $z_x(x,t)$, $z(x,t)$, $Y(t)$ and $m(t)$ are continuous), we have that $V(t_{j+1}^-) = V(t_{j+1})$ and $V(t_j^+) = V(t_j)$, thus

$$V\left(t_{j+1}\right) \leq e^{-\sigma(t_{j+1} - t_j)}V\left(t_j\right). \tag{131}$$

Hence, for any $t \geq 0$ in $t \in \left[t_j, t_{j+1}\right), j \in \mathbb{N}$, by recursion we can also obtain the following:

$$V(t) \leq e^{-\sigma t}V(0). \tag{132}$$

Defining

$$
\begin{aligned}
\Upsilon(t) =& \|\varpi[t]\|^2 + \|\tilde{w}[t]\|^2 + \|\tilde{w}_x[t]\|^2 + \|z_x[t]\|^2 \\
&+ \|z[t]\|^2 + |Y(t)|^2 + |m(t)|,
\end{aligned} \tag{133}
$$

we have $\xi_3\Upsilon(t) \leq V(t) \leq \xi_4\Upsilon(t)$ where $\xi_3 = \min\{\frac{r_0}{2}, 3r_a, r_b, \frac{r_c}{2}, r_d, r_e, 1\} > 0$, $\xi_4 = \max\left\{\frac{r_0}{2}, 3r_a, r_be^{c_1D}, \frac{r_c}{2}, r_de^{c_2D}, r_e, 1\right\} > 0$. Thus we get

$$\Upsilon(t) \leq \frac{\xi_4}{\xi_3}\Upsilon(0)e^{-\sigma t}. \tag{134}$$

Therefore, recalling (101), using (74)–(77), (90)–(92) and (134), we have

$$
\begin{aligned}
\Omega(t) \leq& \left(3q_1 + 2q_2 + 2q_3 + 2\zeta + \frac{3q_1 + q_2 + q_3 + \zeta}{D}\right)\|z[t]\|^2 \\
&+ |m(t)| + (3q_1 + q_2 + 2q_3 + \zeta)(\|\varpi[t]\|^2 + \|z_x[t]\|^2) \\
&+ 2q_4\|\tilde{w}[t]\|^2 + \zeta|Y(t)|^2 \\
\leq& \varrho\Upsilon(t) \leq \varrho\frac{\Upsilon(0)\xi_4}{\xi_3}e^{-\sigma t}
\end{aligned} \tag{135}
$$

where $\varrho = \max\{3q_1 + 2q_2 + 2q_3 + 2\zeta + \frac{3q_1+q_2+q_3+\zeta}{D}, 2q_4\} > 0$. It implies that $\Omega(t)$ is exponentially convergent to zero. Recalling (94) and (135), we can straightforwardly obtain that the proposed event-triggered control input U_d exponentially converges to zero as well. The second property of Theorem 2 is thus obtained.

Remark 2. To avoid the confusion caused by lots of parameters, we sort out the parameters into three categories:
(a) plant parameters: $\lambda, \varepsilon, a_{i,j}$,
(b) design parameters: $\kappa_1, \kappa_2, \kappa_3, \kappa_4, \eta, \xi, \lambda_d, \bar{c}_i$,
(c) analysis parameters: $r_0, r_a, r_b, r_c, r_d, r_e, \delta_0, c_1, c_2$.

All conditions of the these parameters are cascaded rather than coupled. When implementing the controller, it is convenient to solve all conditions of the parameters in the order $\{\bar{c}_i, c_1, \delta_0\} \to \{\kappa_1, \kappa_2, \kappa_3, \kappa_4\} \to \{r_0, r_d\} \to \{r_b, c_2\} \to \{r_e\} \to \{r_a, r_c, \lambda_d\}$ according to (121)–(128), where the positive constants η and ξ are free.

7. Numerical simulations

7.1. Model

In the simulation example, we consider the reaction–diffusion system with $\varepsilon = 1$, $\lambda = 12$ and a second-order actuator ODE with $a_{1,1} = 1$, $a_{2,1} = 0$, $a_{2,2} = 1$, under the initial conditions $u(x,0) = \sin(\pi x)$, $\hat{u}(x,0) = 0$ and $x_1(0) = 0$, $x_2(0) = 0$. The

state delay is set to be $D = 0.5$. For numerical simulations by the finite difference method, both plant and observer states are discretized with uniform step sizes of $\Delta x = 0.05$ for the space variable and $\Delta t = 0.001$ for the time variable.

7.2. Design parameters and gain kernels

The parameters for the event-triggered mechanism are chosen as follows: $m(0) = -5 \times 10^5$, $\xi = 1.8 \times 10^4$, $\eta = 9.775$, $\bar{c}_1 = 235$, and $\bar{c}_2 = 120$. To satisfy (109) and (112), we choose $\kappa_1 = 4.56 \times 10^5$, $\kappa_2 = 758$, $\kappa_3 = 124$, $\kappa_4 = 358$. According to (127), we choose $\lambda_d = 570$.

The kernels $k(x, y)$ and $\alpha(x, y)$ are directly obtained from (21) and (31) (using the modified Bessel function given in Krstic and Smyshlyaev (2008a)). Then $p_1(x)$ given in (22) is obtained by using $\alpha(x, 0)$. The approximate solution of $\gamma(x, y)$ in (32) is obtained by the finite series (n from 1 to 100) and $p(s)$ in (33) is then obtained by calculating the partial derivative of $\gamma(x, y)$ with respect to y.

7.3. Simulation results

The proposed observer-based continuous-in-time control signal $U_f(t)$ defined in (42) is shown in Fig. 3. Applying the controller $U_f(t)$, it is shown in Figs. 4(a) and 4(b) that PDE state $u(x, t)$ and ODE state $X(t)$ are convergent to zero. Next, we test the performance of the event-triggered controller. The event-triggered control input U_d defined in (94), which is in the piecewise-constant form, and the continuous-in-time control signal used in ETM are shown in Fig. 5. The minimal dwell time in this case is $0.002\,s$ (the time step in the simulation is $0.001\,s$). Applying the proposed observer-based event-triggered controller U_d defined in (94), it is shown in Figs. 6(a) and 6(b) that both PDE state $u(x, t)$ and ODE state $X(t)$ are convergent to zero. The evolution of the observer error system $\tilde{u}(x, t)$ is shown in Fig. 7.

Besides, we test the controller with delay $D = 0$, and the results are shown in Figs. 8(a) and 8(b), which illustrate that both PDE state $u(x, t)$ and ODE state $X(t)$ converge to zero as well. Compared to the case subject to delay, the convergence is faster and the overshoot is smaller. The event-triggered control input signal for the case of $D = 0$ is presented in Fig. 9, where the minimal dwell time remains the same as the earlier case.

In addition, to test the robustness of our approach to the delay mismatch, we consider the true delay as 0.55 while the delay D in the controller is set as $D = 0.5$. Resetting the control gains as $\bar{c}_1 = 61.5$, $\bar{c}_2 = 27.5$ and then applying the controller, it is shown in Figs. 10(a), 10(b), and 11 that both PDE and ODE states, as well as the observer error, are exponentially convergent to zero in the presence of such a delay mismatch, even though the convergent rate is slower than the known delay case. From several tests, we find that the robustness to the delay mismatch is around 10% in this simulation case. In our future work, the uncertain delay will be dealt with by incorporating the delay-adaptive design to improve the robustness with respect to the large delay mismatch.

8. Conclusion

In this paper, we have proposed an event-triggered output-feedback boundary control scheme for a class of reaction–diffusion PDE subject to a delayed actuator, where the actuator is modeled by a linear ODE, and the delay is described by a transport PDE. First, we build a state observer for the PDE plant based on a "copy of the plant plus output injections" structure. Based on the observer, we design the continuous-in-time controller by two PDE backstepping transformations together with one n-order ODE backstepping transformation. For the continuous-in-time control

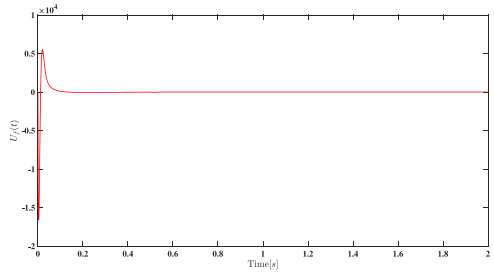

Fig. 3. The observer-based output-feedback continuous-in-time control input signal $U_f(t)$ in (42).

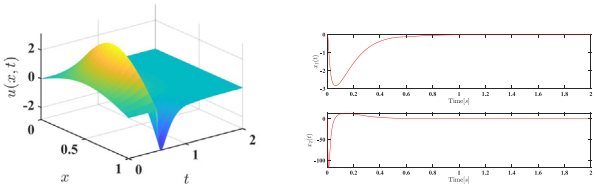

(a) Results for $u(x,t)$. (b) Results for $X(t)$.

Fig. 4. Results under the continuous-in-time control input $U_f(t)$ (42).

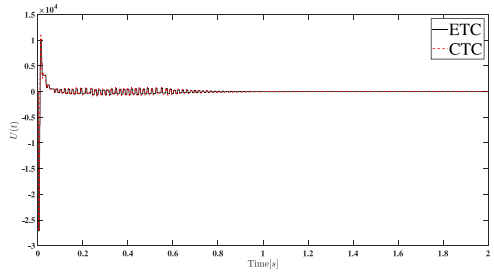

Fig. 5. The event-triggered control input U_d and the continuous-in-time control (CTC) signal used in ETM.

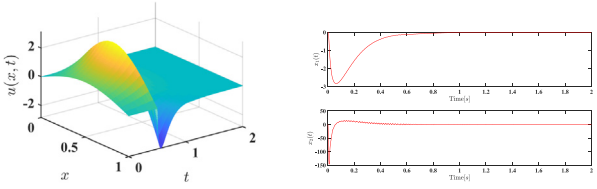

(a) Results for $u(x,t)$. (b) Results for $X(t)$.

Fig. 6. Results under the event-triggered control input U_d (94).

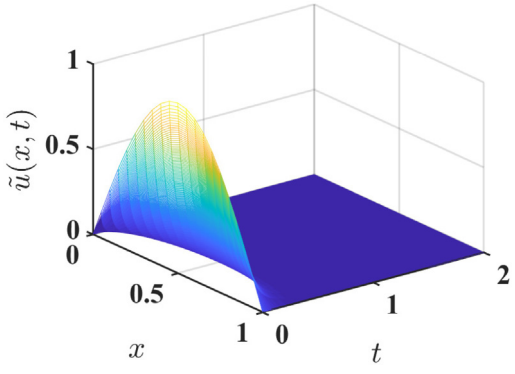

Fig. 7. The evolution of the observer errors $\tilde{u}(x, t)$.

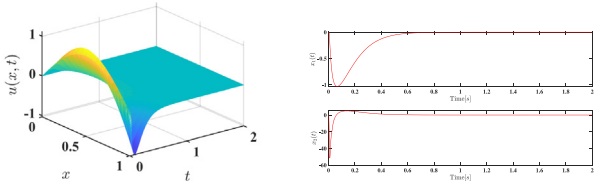

(a) Results for $u(x,t)$. (b) Results for $X(t)$.

Fig. 8. Results under the event-triggered control input U_d in the case of $D = 0$.

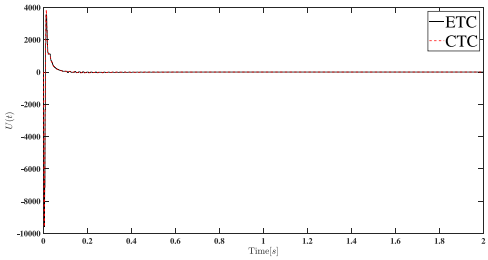

Fig. 9. The event-triggered control input U_d and the continuous-in-time control (CTC) signal used in ETM in the case of $D = 0$.

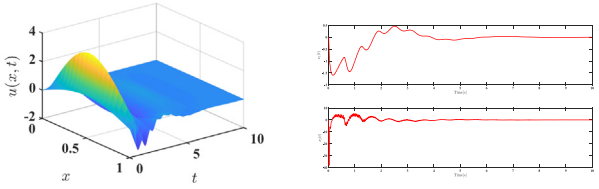

(a) Results for $u(x,t)$. (b) Results for $X(t)$.

Fig. 10. Results under the event-triggered control input U_d in the presence of the delay mismatch (the nominal delay 0.5 and true delay 0.55).

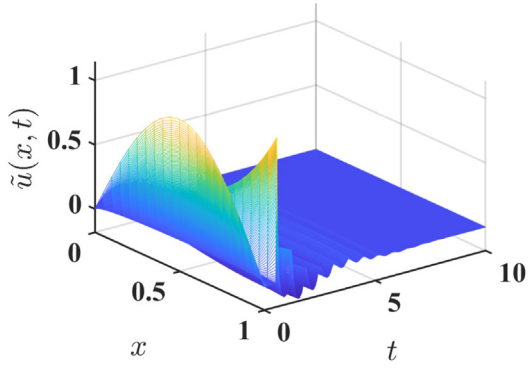

Fig. 11. The evolution of the observer errors $\tilde{u}(x,t)$ under the delay mismatch (the nominal delay 0.5 and true delay 0.55).

input, we then impose an event-triggering the mechanism that determines the update times using the observer and actuator states, the output-feedback event-triggered controller is thus obtained. We have proved that the proposed control guarantees: (1) there exists a minimal dwell-time independent of the initial conditions, which excludes the Zeno behavior; (2) the closed-loop system is well-posed, and all the plant states in the system are exponentially convergent to zero; (3) the event-triggered control signal is convergent to zero. The effectiveness of the proposed design is verified by a numerical example.

In this paper, we only take the known delay into account. In our future work, we will deal with the uncertain delay and expand the current controller to a delay-adaptive type. We also plan to work on reducing the conservatism existing in the design parameter selection to avoid Zeno behavior. Besides, the recent development in Rathnayake, Diagne, Cortés, and Krstic (2025) provides a possible way to reduce the number of updates in the controller, which will also be a part of our future work.

Appendix A. The calculation details in the backstepping transformations (28)–(30)

A.1. Calculation details of (28)

To find out what conditions $k(x,y)$ has to satisfy, we differentiate the transformation (28) with respect to x and t, then from (43), we get

$$\begin{aligned}0 =& \int_0^x (\varepsilon k_{xx}(x,y) - \varepsilon k_{yy}(x,y) - \lambda k(x,y))\hat{u}(y,t)dy \\ &+ \left(\lambda + 2\varepsilon \frac{d}{dx}k(x,x)\right)\hat{u}(x,t) + \varepsilon k(x,0)\hat{u}_x(0,t) \\ &+ \left(p_1(x) - \int_0^x k(x,y)p_1(y)dy\right)\tilde{u}_x(0,t) - g_1(x)\tilde{w}_x(0,t). \end{aligned} \tag{A.1}$$

Differentiating the transformation (20) with respect to x and combining with (24) gives

$$\tilde{u}_x(0,t) = \tilde{w}_x(0,t). \tag{A.2}$$

Considering (A.2) and $g_1(x)$ given by (50), the following three conditions have to be satisfied so that (A.1) is valid for any $\hat{w}(x,t)$:

$$\varepsilon k_{xx}(x,y) - \varepsilon k_{yy}(x,y) - \lambda k(x,y) = 0, \tag{A.3}$$

$$k(x,0) = 0, \tag{A.4}$$

$$\lambda + 2\varepsilon \frac{d}{dx}k(x,x) = 0. \tag{A.5}$$

The explicit solution of $k(x,y)$ is given by (31) which can be obtained following chapter 4 in Krstic and Smyshlyaev (2008a).

A.2. Calculation details of (29)

Differentiating (29) with respect to x and t, then from (46), (14), and (15), one obtains

$$\begin{aligned}0 =& \int_0^1 \left(\gamma_x(x,y) - \lambda\gamma(x,y) - \varepsilon\gamma_{yy}(x,y)\right)\hat{u}(y,t)dy \\ &+ (p(x-1) + \varepsilon\gamma_y(x,1))v(1,t) \\ &- \tilde{u}_x(0,t)\int_0^1 \gamma(x,y)p_1(y)dy - \varepsilon\gamma(x,1)\hat{u}_x(1,t) \\ &+ \varepsilon\gamma(x,0)\hat{u}_x(0,t) - g_2(x)\tilde{w}_x(0,t). \end{aligned} \tag{A.6}$$

Considering (A.2) and $g_2(x)$ given by (51), the kernel $\gamma(x,y)$ is found to satisfy:

$$\gamma_x(x,y) = \varepsilon\gamma_{yy}(x,y) + \lambda\gamma(x,y), \tag{A.7}$$

$$\gamma(x,0) = 0, \tag{A.8}$$

$$\gamma(x,1) = 0 \tag{A.9}$$

with the following condition derived from (45) as

$$\gamma(1,y) = k(1,y). \tag{A.10}$$

After solving for $\gamma(x,y)$, the kernel p is then obtained as

$$p(s) = -\varepsilon\gamma_y(1+s,1), \quad s \in [0,D]. \tag{A.11}$$

The explicit solutions of $\gamma(x,y)$ and $p(s)$ are given by (32) and (33) which can be obtained following chapter 18 in Krstic (2009b).

A.3. Calculation details of (30) and the derivation of $U_f(t)$

Next we show the derivation of (34) and (35) with gains defined in (36)–(41) in the transformation (30), as well as that of the control input (42).

Step.1 Considering (30) at $i = 1$, we directly have $y_1(t) = x_1(t) - \Gamma_0(t)$. Compare with (47), using (11), (29), (30), we derive Γ_0 given by (34).

Step.2 Taking the time derivative of (30) at $i = 1$, recalling (4), one obtains

$$\begin{aligned}\dot{y}_1(t) =&\dot{x}_1(t) - \dot{\Gamma}_0(t)\\ =&(a_{1,1} - p(0))x_1(t) + x_2(t) - \int_0^1 \gamma_x(1+D,y)\hat{u}(y,t)dy\\ &- \int_1^{1+D} p'(1+D-y)v(y,t)dy\\ &- \tilde{u}_x(0,t)\int_0^1 \gamma(1+D,y)p_1(y)dy. \end{aligned} \tag{A.12}$$

Consider (48) at $i = 1$ as well as (30) for $i = 2$, we obtain

$$\begin{aligned}\dot{y}_1(t) =& - \bar{c}_1(x_1(t) - \Gamma_0(t)) - \tilde{u}_x(0,t)\int_0^1 n_{0,1}(y)p_1(y)dy\\ &+ x_2(t) - \Gamma_1(t). \end{aligned} \tag{A.13}$$

Compare (A.12) with (A.13), we can deduce that

$$\begin{aligned}\Gamma_1(t) =& - (a_{1,1} + \bar{c}_1 - p(0))x_1(t)\\ &+ \int_1^{1+D}(p'(1+D-y) + \bar{c}_1 p(1+D-y))v(y,t)dy\\ &+ \int_0^1 (\gamma_x(1+D,y) + \bar{c}_1\gamma(1+D,y))\hat{u}(y,t)dy, \end{aligned} \tag{A.14}$$

i.e., (35) at $i = 1$ with gains given by (36)–(38).

Step. 3 In the previous two steps, we have verified the expressions of Γ_i at $i = 0, 1$ by comparing the original ODE system (12) and the target ODE system (48). Next, we show the recursive form of Γ_i. Based on the original ODE system (12) and the recursive form of functions Γ_i used in the transformation (30), we derive the target ODE system (48), where we verify the expressions of Γ_i at $i = 2, \dots, n-1$. After obtaining Γ_i at $i = 1$, we give a recursive form of Γ_i as

$$\begin{aligned}\Gamma_i(t) =& - \sum_{j=1}^{i} a_{i,j}x_j(t) + \dot{\Gamma}_{i-1}(t) - \bar{c}_i y_i(t)\\ &- \tilde{u}_x(0,t)\int_0^1 n_{i-1,1}(y)p_1(y)dy, \quad 2 \le i \le n-1,\ i \in \mathbb{N}. \end{aligned} \tag{A.15}$$

Then, taking the time derivative of (30), we obtain $\dot{y}_i(t) = \dot{x}_i(t) - \dot{\Gamma}_{i-1}(t)$. Using (4) and (A.15), we get

$$\begin{aligned}\dot{y}_i(t) =& \sum_{j=1}^{i} a_{i,j}x_j(t) + x_{i+1}(t) - \Big(\Gamma_i(t) + \bar{c}_i y_i(t)\\ &+ \sum_{j=1}^{i} a_{i,j}x_j(t) + \tilde{u}_x(0,t)\int_0^1 n_{i-1,1}(y)p_1(y)dy\Big), \end{aligned} \tag{A.16}$$

for $2 \le i \le n-1,\ i \in \mathbb{N}$. Considering (30), we obtain from (A.16) that

$$\dot{y}_i(t) = -\bar{c}_i y_i(t) - \tilde{u}_x(0,t)\int_0^1 n_{i-1,1}(y)p_1(y)dy + y_{i+1}(t), \tag{A.17}$$

i.e., (48) at $i = 2, \dots, n-1$.

Step.4 Using (A.15), by recursion we can derive Γ_{n-1}. We choose the control input as

$$\begin{aligned}U_f(t) =& - \sum_{j=1}^{n} a_{n,j}x_j(t) + \dot{\Gamma}_{n-1}(t) - \bar{c}_n y_n(t)\\ &- \tilde{u}_x(0,t)\int_0^1 n_{n-1,1}(y)p_1(y)dy. \end{aligned} \tag{A.18}$$

Then we obtain from (30) at $i = n$ that

$$\begin{aligned}\dot{y}_n(t) =& \sum_{j=1}^{n} a_{n,j}x_j(t) + U_f(t) - \dot{\Gamma}_{n-1}(t)\\ =& - \bar{c}_n y_n(t) - \tilde{u}_x(0,t)\int_0^1 n_{n-1,1}(y)p_1(y)dy, \end{aligned} \tag{A.19}$$

i.e., (49) (recalling (A.2)).

Step.5 We have verified (35) at $i = 1$ with gains given by (36)–(38) and the recursive form of Γ_i and $U_f(t)$ given by (A.15) and (A.18). Next, we use the recursive form (A.15) and (A.18) to derive Γ_i and $U_f(t)$ expressed by the original states. Using (30) and (35), we can obtain from (A.15)

$$\begin{aligned}\Gamma_{i+1}(t) =& - \sum_{j=1}^{i+1} a_{i+1,j}x_j(t) - \bar{c}_{i+1}(x_{i+1}(t) - \Gamma_i(t))\\ &+ \dot{\Gamma}_i(t) - \tilde{u}_x(0,t)\int_0^1 n_{i,1}(y)p_1(y)dy\\ =& - (a_{i+1,i+1} + \bar{c}_{i+1})x_{i+1}(t) - \sum_{j=1}^{i} a_{i+1,j}x_j(t)\\ &+ M_i^T\dot{\underline{x}}_i(t) - (a_{i,i} + \bar{c}_i)\dot{x}_i(t)\\ &+ \int_0^1 n_{i,1}(y)\hat{u}_t(y,t)dy + \int_1^{1+D} n_{i,2}(y)v_t(y,t)dy\\ &+ \bar{c}_{i+1}\Big(-(a_{i,i} + \bar{c}_i)x_i(t) + M_i^T\underline{x}_i(t)\\ &+ \int_0^1 n_{i,1}(y)\hat{u}(y,t)dy + \int_1^{1+D} n_{i,2}(y)v(y,t)dy\Big)\\ &- \tilde{u}_x(0,t)\int_0^1 n_{i,1}(y)p_1(y)dy, \end{aligned} \tag{A.20}$$

for $i \le n-2,\ i \in \mathbb{N}$. Recalling (7)–(12), we can further derive Γ_{i+1} expressed by the original states by (A.20) and compare it with (35) at $i+1$, we get (39)–(41) for $i \le n-2$.

Step.6 After solving for Γ_{n-1} by recursion, the controller U_f is obtained from (A.18) given by

$$\begin{aligned}U_f(t) =&(-a_{n,n} - \bar{c}_n)x_n(t) + \int_0^1 n_{n,1}(y)\hat{u}(y,t)dy\\ &+ \int_1^{1+D} n_{n,2}(y)v(y,t)dy + M_n^T X(t) \end{aligned} \tag{A.21}$$

where the kernel gains $n_{n,1}(y)$, $n_{n,2}(y)$, M_n^T are given by the bases (36)–(38) and recursive formulas (39)–(41).

Appendix B. Proof of Lemma 2

For the ϖ-subsystem we have that

$$\frac{d}{dt}\frac{1}{2}\|\varpi[t]\|^2 = -\varepsilon\|\varpi_x[t]\|^2 + \tilde{w}_x(0,t)\int_0^1 g_1(x)\varpi(x,t)dx$$

$$- (\tilde{w}_x(0,t)g_2(1) + z_x(1,t)) \int_0^1 x\varpi(x,t)dx. \quad \text{(B.1)}$$

Recalling (55), based on the Wirtinger's inequality we have $-\varepsilon\|\varpi_x[t]\|^2 \le -\frac{\pi^2\varepsilon}{4}\|\varpi[t]\|^2$. Then using Cauchy–Schwarz inequality, we derive from (B.1) that

$$\begin{aligned}\frac{d}{dt}\frac{1}{2}\|\varpi[t]\|^2 \le& -\frac{\pi^2\varepsilon}{4}\|\varpi[t]\|^2 + \left(\int_0^1 g_1(x)^2dx\right)^{\frac{1}{2}}|\tilde{w}_x(0,t)|\\ &\times \|\varpi[t]\| + |g_2(1)\tilde{w}_x(0,t) + z_x(1,t)|\\ &\times \left(\int_0^1 x^2dx\right)^{\frac{1}{2}}\|\varpi[t]\|. \quad \text{(B.2)}\end{aligned}$$

Then we derive (68) from (B.2) based on Young's equality.

For the $\tilde{w}$-subsystem, we can easily derive (69) and (70) applying integration by parts. Next, we prove (71). According to $\int_0^x \tilde{w}_y(y,t)\tilde{w}_{yy}(y,t)dy = \frac{1}{2}\tilde{w}_x^2(x,t) - \frac{1}{2}\tilde{w}_x^2(0,t)$, we have

$$\begin{aligned}\tilde{w}_x(0,t)^2 =& \tilde{w}_x(x,t)^2 + 2\int_0^x \tilde{w}_y(y,t)\tilde{w}_{yy}(y,t)dy\\ \le& \tilde{w}_x(x,t)^2 + 2\int_0^1 |\tilde{w}_x(x,t)||\tilde{w}_{xx}(x,t)|dx.\end{aligned}$$

That is, $\int_0^1 \tilde{w}_x(0,t)^2dx \le \int_0^1(\|\tilde{w}_x[t]\|^2 + \|\tilde{w}_{xx}[t]\|^2)dx + \int_0^1 \tilde{w}_x(x,t)^2dx$, then we get (71). According to (57) and (58), applying integration by parts, we obtain

$$\begin{aligned}&\frac{d}{dt}\int_1^{1+D} e^{c_1(x-1)}z_x^2(x,t)dx\\ &= e^{c_1D}(\dot{y}_1(t) - g_2(1+D)\tilde{w}_x(0,t))^2 - z_x^2(1,t)\\ &- c_1\int_1^{1+D} e^{c_1(x-1)}z_x^2(x,t)dx\\ &+ 2\int_1^{1+D} e^{c_1(x-1)}z_x(x,t)\tilde{w}_x(0,t)g_2'(x)dx, \quad \text{(B.3)}\\ &\frac{d}{dt}\int_1^{1+D} e^{c_2(x-1)}z^2(x,t)dx\\ &= e^{c_2D}y_1^2(t) - z^2(1,t) - c_2\int_1^{1+D} e^{c_2(x-1)}z^2(x,t)dx\\ &+ 2\int_1^{1+D} e^{c_2(x-1)}z(x,t)\tilde{w}_x(0,t)g_2(x)dx. \quad \text{(B.4)}\end{aligned}$$

Applying the Cauchy–Schwarz inequality into (B.3) and (B.4), we derive (72) and (73). Applying the Cauchy–Schwarz inequality into (61) and (62),we then obtain (74) and (75), where $q_1 = 4\max\left\{\left(1 + (\int_0^1\int_0^x l(x,y)^2dydx)^{\frac{1}{2}}\right)^2, \frac{1}{3}\left(1 + \int_0^1\int_0^x l(x,y)^2dydx\right)\right\}$, $q_2 = 3\max\left\{2(1 + (\int_1^{1+D}\int_1^x q(x-y)^2dydx)^{\frac{1}{2}})^2, \int_1^{1+D}\int_0^1 \gamma^I(x,y)^2dydx, \int_1^{1+D}(\int_0^1 y\gamma^I(x,y)dy)^2dx\right\}$. Taking the spatial derivative of (62), we obtain

$$\begin{aligned}v_x(x,t) =& z_x(x,t) + \int_1^x q'(x-y)z(y,t)dy + q(0)z(x,t)\\ &+ \int_0^1 \gamma_x^I(x,y)\varpi(y,t)dy + z(1,t)\int_0^1 y\gamma_x^I(x,y)dy. \quad \text{(B.5)}\end{aligned}$$

Applying the Cauchy–Schwarz inequality into (B.5), we then obtain (76), where $q_3 = 4\max\left\{\int_1^{1+D}\int_0^1 \gamma_x^I(x,y)^2dydx, \int_1^{1+D}(\int_0^1 y\gamma_x^I(x,y)dy)^2dx, 2\left(q_0 + (\int_1^{1+D}\int_1^x q'(x-y)^2dydx)^{\frac{1}{2}}\right)^2\right\}$. Applying the Cauchy–Schwarz inequality into (63), recalling (34) and (35), we get

$$x_1(t)^2 \le h_0(y_1(t)^2 + \|\hat{u}[t]\|^2 + \|v[t]\|^2), \quad \text{(B.6)}$$

$$x_{i+1}(t)^2 \le h_i(y_{i+1}(t)^2 + \|\hat{u}[t]\|^2 + \|v[t]\|^2 + |\underline{x}_i(t)|^2) \quad \text{(B.7)}$$

for $i \le n-1$, $i \in \mathbb{N}^*$, where $h_0 = 3\max\left\{\int_0^1 \gamma(1+D,y)^2dy, \int_1^{1+D} p(1+D-y)^2dy\right\}$, $h_i = 4\max\left\{\int_0^1 n_{i,1}^2(y)dy, \int_1^{1+D} n_{i,2}^2(y)dy, |M_i^T - (a_{i,i} + \bar{c}_i)e_{i,i}^T|^2\right\}$. Therefore, we obtain

$$\begin{aligned}|\underline{x}_i(t)|^2 \le& \sum_{j=0}^{i-1} h_j(y_{j+1}(t)^2 + \|\hat{u}[t]\|^2 + \|v[t]\|^2)\\ &+ \sum_{j=1}^{i-1} h_j|\underline{x}_j(t)|^2. \quad \text{(B.8)}\end{aligned}$$

That is,

$$|\underline{x}_i(t)|^2 \le H_i(\underline{y}_i(t)^2 + \|\hat{u}[t]\|^2 + \|v[t]\|^2), \quad \text{(B.9)}$$

where $H_1 = h_0$, and $H_i = \sum_{j=0}^{i-1} h_j + \sum_{j=1}^{i-1} h_jH_j$ for $i \le n, i \in \mathbb{N}^*$. Furthermore, recalling (74) and (75),we get (77) where $\zeta = H_n(q_1 + q_2)$.

References

Argomedo, F. B., Witrant, E., & Prieur, C. (2014). *Safety factor profile control in a Tokamak*. Springer.

Auriol, J., Aarsnes, U. J. F., Martin, P., & Di Meglio, F. (2018). Delay-robust control design for two heterodirectional linear coupled hyperbolic PDEs. *IEEE Transactions on Automatic Control*, *63*(10), 3551–3557.

Auriol, J., Bribiesca Argomedo, F., Saba, D. B., Di Loreto, M., & Di Meglio, F. (2018). Delay-robust stabilization of a hyperbolic PDE-ODE system. *Automatica*, *95*, 494–502.

Baccoli, A., Pisano, A., & Orlov, Y. (2015). Boundary control of coupled reaction–diffusion processes with constant parameters. *Automatica*, *54*, 80–90.

Burns, J. A., Herdman, T. L., & Zietsman, L. (2013). Approximating parabolic boundary control problems with delayed actuator dynamics. In *2013 American control conference* (pp. 2080–2085).

Chen, Guangwei, Vazquez, Rafael, Liu, Zhitao, & Su, Hongye (2023). Backstepping control of an underactuated hyperbolic–parabolic coupled PDE system. *IEEE Transactions on Automatic Control*, *69*(2), 1218–1225.

Desvillettes, L., Fellner, K., & Bao, T. (2017). Trend to equilibrium for reaction-diffusion systems arising from complex balanced chemical reaction networks. *SIAM Journal on Mathematical Analysis*, *49*, 2666–2709.

Deutscher, J., & Gehring, N. (2020). Output feedback control of coupled linear parabolic ODE–PDE–ODE systems. *IEEE Transactions on Automatic Control*, *66*(10), 4668–4683.

Deutscher, Joachim, Gehring, Nicole, & Jung, Nick (2023). Backstepping control of coupled general hyperbolic-parabolic PDE-PDE systems. *IEEE Transactions on Automatic Control*.

Diagne, M., Bekiaris-Liberis, N., Otto, A., & Krstic, M. (2017a). Compensation of input delay that depends on delayed input. *Automatica*, *85*, 362–373.

Diagne, M., Bekiaris-Liberis, N., Otto, A., & Krstic, M. (2017b). Control of transport PDE/Nonlinear ODE cascades with state-dependent propagation speed. *IEEE Transactions on Automatic Control*, *62*, 6278–6293.

Diagne, M., & Karafyllis, I. (2021). Event-triggered boundary control of a continuum model of highly re-entrant manufacturing systems. *Automatica*, *134*, Article 109902.

Donkers, M. C. F., & Heemels, W. P. M. H. (2012). Output-based event-triggered control with guaranteed L_∞-gain and improved and decentralized event-triggering. *IEEE Transactions on Automatic Control*, *57*(6), 1362–1376.

Espitia, N. (2020). Observer-based event-triggered boundary control of a linear 2×2 hyperbolic systems. *Systems & Control Letters*, *138*, Article 104668.

Espitia, N., Auriol, J., Yu, H., & Krstic, M. (2022). Traffic flow control on cascaded roads by event-triggered output feedback. *International Journal of Robust and Nonlinear Control*, *32*, 5919–5949.

Espitia, N., Girard, A., Marchand, N., & Prieur, C. (2018). Event-based boundary control of a linear 2×2 hyperbolic system via backstepping approach. *IEEE Transactions on Automatic Control*, *63*(8), 2686–2693.

Espitia, N., Karafyllis, I., & Krstic, M. (2021). Event-triggered boundary control of constant-parameter reaction–diffusion PDEs: A small-gain approach. *Automatica*, *128*, Article 109562, URL https://www.sciencedirect.com/science/article/pii/S0005109821000820.

Grindrod, P. (1991). *Patterns and waves: The theory and application of reaction-diffusion equations*. USA: Oxford University Press.

Heemels, W. P. M. H., Donkers, M. C. F., & Teel, Andrew R. (2013). Periodic event-triggered control for linear systems. *IEEE Transactions on Automatic Control*, *58*(4), 847–861.

Holmes, E., Lewis, M. A., Banks, J., & Veit, D. (1994). Partial differential equations in ecology: Spatial interactions and population dynamics. *Ecology*, *75*, 17–29.

Ivancevic, V., & Ivancevic, T. (2008). Ricci flow and nonlinear reaction–diffusion systems in biology, chemistry, and physics. *Nonlinear Dynamics*, *65*.

Karafyllis, I., & Krstic, M. (2019). *Input-to-state stability for PDEs*. Springer.

Katz, R., Fridman, E., & Selivanov, A. (2021). Boundary delayed observer-controller design for reaction–diffusion systems. *IEEE Transactions on Automatic Control*, *66*(1), 275–282.

Koga, S., Bresch-Pietri, D., & Krstic, M. (2020). Delay compensated control of the Stefan problem and robustness to delay mismatch. *International Journal of Robust and Nonlinear Control*, *30*, 2304–2334.

Koga, S., Demir, C., & Krstic, M. (2023). Event-triggered safe stabilizing boundary control for the stefan PDE system with actuator dynamics. In *2023 American control conference* (pp. 1794–1799).

Koudohode, F., Espitia, N., & Krstic, M. (2024). Event-triggered boundary control of an unstable reaction diffusion PDE with input delay. *Systems & Control Letters*, *186*, Article 105775.

Krener, A. J. (2022). Optimal boundary control of a nonlinear reaction diffusion equation via completing the square and Al'brekht's method. *IEEE Transactions on Automatic Control*, *67*(12), 6698–6709.

Krstic, M. (2009a). Control of an unstable reaction–diffusion PDE with long input delay. *Systems & Control Letters*, *58*(10–11), 773–782.

Krstic, M. (2009b). Delay compensation for nonlinear, adaptive, and PDE systems. Springer,

Krstic, M., & Smyshlyaev, A. (2008a). *Boundary control of PDEs*. Philadelphia, PA: Society for Industrial and Applied Mathematics.

Krstic, M., & Smyshlyaev, A. (2008b). Adaptive boundary control for unstable parabolic PDEs—Part i: Lyapunov design. *IEEE Transactions on Automatic Control*, *53*(7), 1575–1591.

Lhachemi, H., & Shorten, R. (2023). Output feedback stabilization of an ODE-reaction–diffusion PDE cascade with a long interconnection delay.. *Automatica*, *147*, Article 110704.

Lhachemi, H., Shorten, R., & Prieur, C. (2019). Control law realification for the feedback stabilization of a class of diagonal infinite-dimensional systems with delay boundary control. *IEEE Control Systems Letters*, *3*(4), 930–935.

Li, J., Wu, Z., & Wen, C. (2021). Adaptive stabilization for a reaction–diffusion equation with uncertain nonlinear actuator dynamics. *Automatica*, *128*, Article 109594.

Marchand, N., Durand, S., & Castellanos, J. F. G. (2013). A general formula for event-based stabilization of nonlinear systems. *IEEE Transactions on Automatic Control*, *58*(5), 1332–1337.

Nagahara, K., & Yanagida, E. (2018). Maximization of the total population in a reaction–diffusion model with logistic growth. *Calculus of Variations and Partial Differential Equations*, *57*.

Postoyan, R., Tabuada, P., Nešić, D., & Anta, A. (2015). A framework for the event-triggered stabilization of nonlinear systems. *IEEE Transactions on Automatic Control*, *60*(4), 982–996.

Rathnayake, B., & Diagne, M. (2023b). Observer-based periodic event-triggered boundary control of the one-phase Stefan problem. *IFAC-PapersOnLine*, *56*(2), 11415–11422.

Rathnayake, B., & Diagne, M. (2023c). Periodic event-triggered boundary control of a class of reaction-diffusion PDEs. In *American Control Conference*. http://dx.doi.org/10.23919/ACC55779.2023.10156485.

Rathnayake, B., & Diagne, M. (2024). Observer-based periodic event-triggered and self-triggered boundary control of a class of parabolic PDEs. *IEEE Transactions on Automatic Control*, *69*(12), 8836–8843.

Rathnayake, B., Diagne, M., Cortés, J., & Krstic, M. (2025). Performance-barrier event-triggered control of a class of reaction-diffusion PDEs. *Automatica*, *174*, Article 112181.

Rathnayake, B., Diagne, M., Espitia, N., & Karafyllis, I. (2022). Observer-based event-triggered boundary control of a class of reaction–diffusion PDEs. *IEEE Transactions on Automatic Control*, *67*(6), 2905–2917.

Rathnayake, B., Diagne, M., & Karafyllis, I. (2022). Sampled-data and event-triggered boundary control of a class of reaction–diffusion PDEs with collocated sensing and actuation. *Automatica*, *137*, Article 110026.

Wang, S., Diagne, M., & Qi, J. (2021). Delay-adaptive predictor feedback control of reaction-advection-diffusion PDEs with a delayed distributed input. *IEEE Transactions on Automatic Control*, *67*, 3762–3769.

Wang, J., & Krstic, M. (2020). Delay-compensated control of sandwiched ODE–PDE–ODE hyperbolic systems for oil drilling and disaster relief. *Automatica*, *120*, Article 109131.

Wang, J., & Krstic, M. (2022a). Delay-compensated event-triggered boundary control of hyperbolic PDEs for deep-sea construction. *Automatica*, *138*, Article 110137.

Wang, J., & Krstic, M. (2022b). Event-triggered adaptive control of a parabolic PDE-ODE cascade with piecewise-constant inputs and identification. *IEEE Transactions on Automatic Control*, 1–16.

Wang, J., & Krstic, M. (2022c). Event-triggered output-feedback backstepping control of sandwich hyperbolic PDE systems. *IEEE Transactions on Automatic Control*, *67*(1), 220–235.

Wang, J., & Krstic, M. (2023). Event-triggered adaptive control of coupled hyperbolic PDEs with piecewise-constant inputs and identification. *IEEE Transactions on Automatic Control*, *68*(3), 1568–1583.

Wang, S., Qi, J., & Diagne, M. (2021). Adaptive boundary control of reaction–diffusion PDEs with unknown input delay. *Automatica*, *134*, Article 109909.

Zhang, P., Liu, T., & Jiang, Z. (2021). Event-triggered stabilization of a class of nonlinear time-delay systems. *IEEE Transactions on Automatic Control*, *66*(1), 421–428.

Zhu, Y., Krstic, M., & Su, H. (2018). PDE boundary control of multi-input LTI systems with distinct and uncertain input delays. *IEEE Transactions on Automatic Control*, *63*(12), 4270–4277.

Hongpeng Yuan received the B.Eng. degree in Automation from University of Science and Technology of China, Hefei, China, in 2022. He is currently pursuing his Ph.D. degree in Control Theory and Control Engineering at Xiamen University, Xiamen, China. His research interests include control of distributed parameter systems, event-triggered control, and delay compensation.

Ji Wang is currently an associate professor in the Department of Automation at Xiamen University, Xiamen, China. He received the Ph.D. degree in Mechanical Engineering in 2018 from Chongqing University, Chongqing, China. From 2019 to 2021, he was a postdoctoral scholar in the Department of Mechanical and Aerospace Engineering at University of California, San Diego, La Jolla, CA, USA. Since 2021, he serves as Associate Editor of Systems & Control Letters. He has coauthored (with M. Krstic) the book entitled *PDE Control of String-Actuated Motion* (Princeton University Press).

Jianping Zeng received his Ph.D. degree from Beihang University in 2000. From 2001 to 2002, he was a postdoctoral scholar at Peking University. He is currently a full professor in the Department of Automation at Xiamen University. He received the Xiamen Science and Technology Progress Award in 2011. His research interests include robust control, nonlinear systems, flight control systems, and motion control technology.

Weiyao Lan received the B.S. degree in precision instrument from Chongqing University, Chongqing, China, in 1995, the M.S. degree in control theory and control engineering from Xiamen University, Xiamen, China, in 1998, and the Ph.D. degree in automation and computer aided engineering from the Chinese University of Hong Kong, Hong Kong SAR, China, in 2004. From 2004 to 2006, he was a Research Fellow with the Department of Electrical and Computer Engineering, National University of Singapore, Singapore. Since December in 2006, he has been with the Department of Automation, Xiamen University, where he is currently a Professor. His research interests include nonlinear control theory and applications, intelligent control technology, and robust and optimal control. Dr. Lan is a Member of Technical Committee on Control Theory, Chinese Associate of Automation. He is serving as an Associate Editor for the Transactions of the Institute of Measurement and Control.